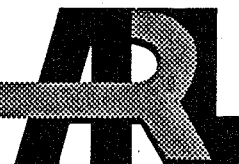ARMY RESEARCH LABORATORY

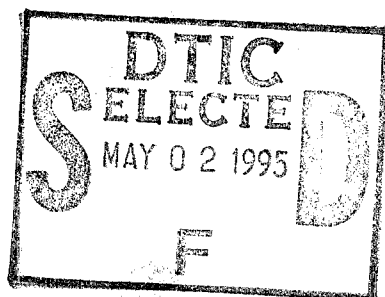# The Effects of Large and Small Scale Turbulence on Sound Propagation in the Atmosphere

by John M. Noble
Harry J. Auvermann
Battlefield Environment Directorate

ARL-TR-565

March 1995

DTIC
ELECTE
MAY 0 2 1995
F

19950501 017

NOTICES

Disclaimers

The findings in this report are not to be construed as an official Department of the Army position, unless so designated by other authorized documents.

The citation of trade names and names of manufacturers in this report is not to be construed as official Government indorsement or approval of commercial products or services referenced herein.

Destruction Notice

When this document is no longer needed, destroy it by any method that will prevent disclosure of its contents or reconstruction of the document.

REPORT DOCUMENTATION PAGE

1. AGENCY USE ONLY (Leave blank)	2. REPORT DATE March 1995	3. REPORT TYPE AND DATES COVERED

4. TITLE AND SUBTITLE

The Effects of Large and Small Scale Turbulence on Sound Propagation in the Atmosphere

5. FUNDING NUMBERS

6. AUTHOR(S)

John M. Noble and Harry J. Auvermann

7. PERFORMING ORGANIZATION NAME(S) AND ADDRESS(ES)

U.S. Army Research Laboratory
Battlefield Environment Directorate
Attn: AMSRL-BE
White Sands Missile Range, NM 88002-5501

8. PERFORMING ORGANIZATION REPORT NUMBER

ARL-TR-565

9. SPONSORING / MONITORING AGENCY NAME(S) AND ADDRESS(ES)

U.S. Army Research Laboratory
2800 Powder Mill Road
Adelphi, MD 20783-1145

10. SPONSORING / MONITORING AGENCY REPORT NUMBER

ARL-TR-565

11. SUPPLEMENTARY NOTES

12a. DISTRIBUTION / AVAILABILITY STATEMENT
Approved for public release; distribution is unlimited.

12b. DISTRIBUTION CODE

Distribution A

13. ABSTRACT (Maximum 200 words)

Propagation of acoustic waves in the atmosphere is affected by several mechanisms. Two of the effects are the scattering of sound by small-scale atmospheric turbulence and fluctuation of the speed of sound gradients by the passage of large-scale atmospheric turbulence. Small- and large-scale atmospheric turbulence causes the acoustic waves to be altered by different mechanisms. Until recently, the majority of work in turbulence effect on accoustics has concentrated on the small-scale turbulence regime of the inertial subrange of the Kolmogorov spectrum. Earlier small-scale turbulence models have concentrated on the statistical-based work of Tatarski. Current turbulence models deal more with the structural nature of the turbulence because the statistical approach does not account for all of the turbulence effects being measured during acoustic propagation experiments. The large-scale turbulence problem cannot be handled very well with a statistical approach to atmospheric turbulence because the regime of the large-scale turbulence extends into the energy containing subrange or sometimes referred to as the source region. This report discusses the current and past turbulence models used to treat the effect of small- and large-scale turbulence on atmospheric acoustic propagation.

14. SUBJECT TERMS

acoustics, turbulence, atmosphere, scattering

15. NUMBER OF PAGES
70

16. PRICE CODE

17. SECURITY CLASSIFICATION OF REPORT	18. SECURITY CLASSIFICATION OF THIS PAGE	19. SECURITY CLASSIFICATION OF ABSTRACT	20. LIMITATION OF ABSTRACT
Unclassified	Unclassified	Unclassified	SAR

Contents

Figures

Tables

2

1. Introduction

The propagation of sound waves close to the ground is a complex problem involving many interesting mechanisms. In addition to geometrical spreading and molecular absorption, which are reasonably well understood, the three main mechanisms that influence the acoustic field are reflection with phase change due to the finite impedance of the ground, refraction by wind and temperature gradients, and scattering by atmospheric turbulence. Outdoor sound propagation in a turbulent medium is not a well-understood process and has only recently begun to receive serious attention.

The effects of turbulent scatter of the acoustic wave in the atmosphere will impact the detectability range and the accuracy of the tracking of tactical targets as passive acoustic sensor arrays are integrated into the battlefield. The effects of turbulent scatter are not new in the tactical sensor arena. The infrared, laser, radar, and millimeter wave sensors also suffer from scattering by atmospheric turbulence. Scattering of the acoustic wave by atmospheric turbulence can assist in the detection of tactical targets by scattering sound into refractive shadow zones. Acoustic sensors allow passive and nonline-of-sight detection of targets. Early warnings of the presence of tactically important targets in the battlefield can be made, so actions can be carried out to destroy the targets before they can destroy your assets.

The negative effect of the scattering by atmospheric turbulence is the impact on the bearing accuracy of passive acoustic sensor arrays. In the presence of large-scale turbulence, the signal at the sensor will fade in and out, making it difficult to keep track of a target. In the presence of the small-scale turbulence, the scattering of the acoustic signal will cause a reduction in the coherence between any two spatial points. The loss in coherence reduces the bearing accuracy of the sensor array causing an increase in the angular region of the location of the target. The need for computer models to predict these effects of atmospheric turbulence, both large and small scale, on propagation of acoustic waves in the atmosphere over long ranges (R > 5 km) is very important.

The aim of this report is to describe some of the effects of large- and small-scale turbulence on sound propagation over ranges less than 1 km. The report will discuss some of the predictive models for the effect of turbulence on sound propagation.

First, the actual sizes for the large- and small-scale of turbulence, which are important to atmospheric acoustics, must be defined. Turbulence arises from instabilities at large Reynolds numbers in flows that are originally laminar. Laminar flow becomes turbulent at a Reynolds number of approximately 2000. [1] Reynolds numbers are estimated by

$$r = \frac{uL_S}{v} \tag{1}$$

where

u =   wind speed
L_S =   the length scale of the motion
v =   the kinematic viscosity of the medium, which is given by the absolute viscosity divided by the density (η/ρ).

The absolute viscosity is 1.84×10^{-5} kg m^{-1} s^{-1} and the density is 1.21 kg m^{-3} for dry air at standard temperature and pressure, giving a kinematic viscosity of 1.5×10^{-5} m^2 s^{-1}. Turbulent flow would begin at wind speeds as little as 0.03 m s^{-1} for a scale length of 1 m, meaning that turbulence is always present in the atmosphere.

A set of eddies is created as soon as a disturbance occurs. These eddies have characteristic lengths and velocities of a lower order than the corresponding geometrical and kinematical quantities of the mean flow. The energy for the entire motion lies in the mean flow, which is distributed over the largest eddies. Turbulence cannot maintain itself because of viscous losses and depends on its environment to obtain energy. A common source of energy for turbulent velocity fluctuations is shear in the mean flow.

Meteorologists divide the motions of the atmosphere into three regimes: macroscale, mesoscale, and microscale. [2] The macroscale motions are those resolved by the synoptic observing network and seen on weather maps. The

4

mesoscale motions occur in horizontal sizes of 10 to 500 km, including such phenomena as sea breezes, mountain-valley wind systems, squall lines, cloud clusters, and many orographic features including standing waves. The microscale motions are all those that are smaller still, and usually the term microscale refers to small-scale waves or to the turbulent part of the flow.

The distribution of the energy of the motion or the variance of other meteorological variables in these regimes is best revealed by spectra. Figure 1 shows a typical energy spectrum for the atmosphere. [3] The region of the energy spectrum most important for outdoor sound propagation is for time scales of turbulence, which occur on the order of 1 hr and less. This time span is associated with microscale and part of the mesoscale regimes.
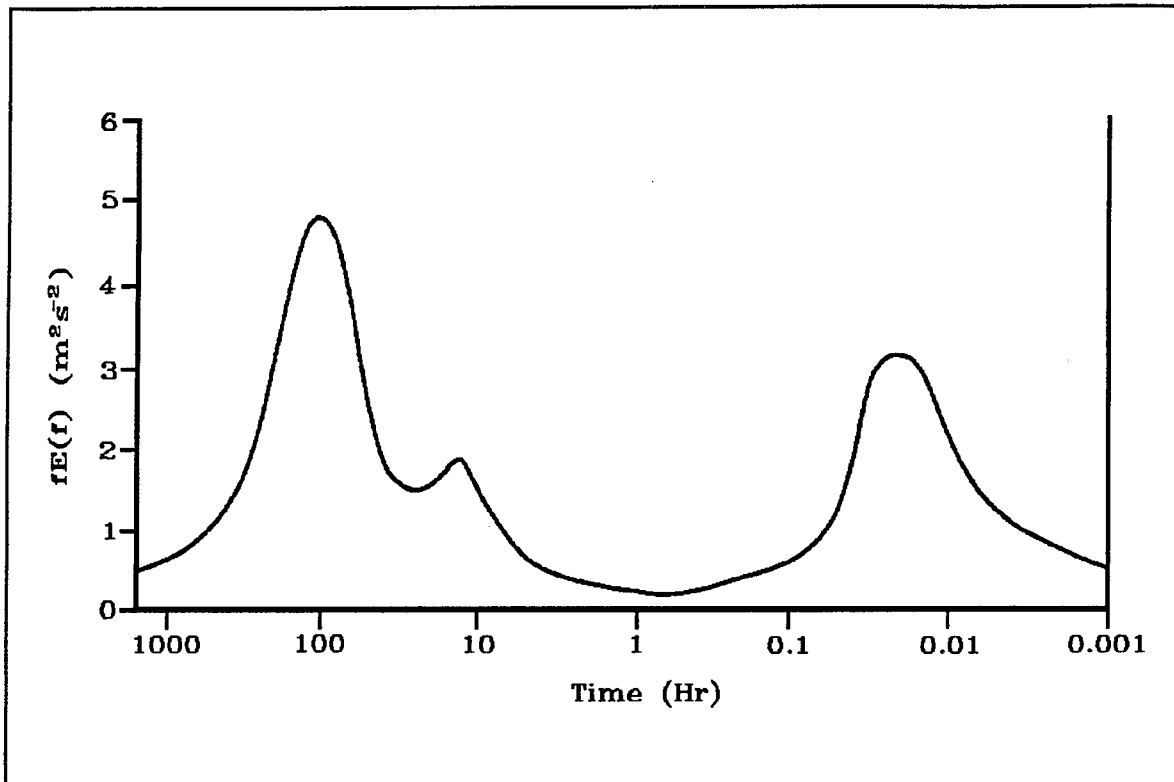
Figure 1. Typical energy spectrum for the atmosphere.

The microscale region of the spectra is typically divided into three portions: energy-containing subrange, inertial subrange, and dissipation subrange, as originally proposed by Kolmogorov. Most of the energy and energy input is

in the energy-containing subrange. Length scales of turbulence in this region are typically tens of meters to several kilometers; local time scales vary between tens of seconds and tens of minutes. The characteristics of spectral densities in this range depend on many variables; wind, roughness, depth of boundary layer, and so on. Wavelengths less than tens of meters, but larger than the Kolmogorov microscale define the inertial subrange. Here no energy enters the system from outside, nor is any energy dissipated. Energy arrives from small wave numbers (larger turbules) and is transmitted toward larger wave numbers (smaller turbules). In the case of the velocity components, the energy leaves the inertial subrange at a rate ϵ. Wavelengths less than the Kolmogorov microscale comprise the dissipation subrange.

Generally, the definition of large-scale turbulence is the turbulence found in the energy-containing subrange, also known as the source subrange. Turbulence in this region is on the order of tens of meters to kilometers. Small-scale turbulence refers to the turbulence found in the inertial subrange. For the purpose of acoustics, small-scale turbulence refers to scale sizes on the order of tens of centimeters to a few meters. This is the definition being used whenever small- or large-scale turbulence is referred to in this report.

2. Small-Scale Turbulence

Much of the statistical work on turbulence effects in acoustics has been done by Chernov, [4] Tatarski, [5] and Karavainikov. [6] Daigle et al. [7] extracted the small-scale turbulence calculations for a spherical wave from Karavainikov to compare to their experimental results. Much of the analyses of turbulent effects has concentrated primarily on the effects of small-scale turbulence on sound propagation through the atmosphere.

2.1 Acoustic Refractive Index Structure Function

The index of refraction n at a point in space can be written as $n = 1 + \mu = c_o / c$ where c_o is the sound speed at reference temperature T_o in the absence of turbulence and μ is the fluctuating part of the acoustic index of refraction for the medium. The sound speed will generally depend on the local temperature T

$$c(T) = c_o \sqrt{\frac{T}{T_o}} \ .$$

(2)

The effects of the local mean wind speed u can be incorporated by

$$c = c(T) + \vec{u} \cdot \hat{r}$$

(3)

where the second term is the dot product between the wind velocity and the unit vector in the direction of sound propagation. Substituting the definition of a dot product yields

$$c = c(T) + u \cos\theta$$

(4)

where θ is the angle between the direction of propagation and the direction toward which the wind blows. Assuming that the variables (T, u) in equation (4) can be written as the sum of the mean value ($<T>, <u>$) and the fluctuation about the mean ($\delta T, \delta u$), equation (4) can be rewritten using the binomial expansion as

$$c = c(\langle T \rangle) \left(1 + \frac{\delta T}{2\langle T \rangle}\right) + \langle u \rangle \cos\theta \left(1 + \frac{\delta u}{\langle u \rangle}\right). \tag{5}$$

Squaring both sides and performing a time average yields, using the concept of the mean for the sound speed ($<c>$) and the fluctuation about the mean (δc):

$$\langle \delta c^2 \rangle = \frac{c_o^2}{4\langle T \rangle^2} \langle \delta T^2 \rangle + \cos^2\theta \langle \delta u^2 \rangle \tag{6}$$

where the time average of the fluctuations are assumed to be zero, or $\langle \delta T \rangle = \langle \delta u \rangle = 0$ has been used, and the cross terms between u and T are assumed to be negligible. The variance of the index of refraction fluctuations $\langle \mu^2 \rangle$ is easily calculated. Using the fact that $\mu = (c_o - c) / c = \delta c/c$, then squaring and taking a timed average results in

$$\langle \mu^2 \rangle = \frac{\langle \delta c^2 \rangle}{c_o^2} \tag{7}$$

where $<c^2>$ has been approximated by c_0^2. Therefore, equation (6) becomes, after dividing by c_0^2 and writing $<\delta u^2> = \sigma_v^2$, $<\delta T^2> = \sigma_T^2$:

$$\langle \mu^2 \rangle = \frac{\sigma_V^2 \cos^2\theta}{c_o^2} + \frac{\sigma_T^2}{4\langle T \rangle^2}. \tag{8}$$

This is the equation for the acoustic refractive index structure function. Equation (8) can be rewritten in the form:

$$C_N^2 = \frac{C_V^2}{c_o^2} + \frac{C_T^2}{4\langle T \rangle^2} \tag{9}$$

where C_V^2 is the mechanical turbulence structure function defined by

$$C_V^2 = \sigma_V^2 \cos^2 \theta = \frac{\langle (\Delta u)^2 \rangle}{r^{2/3}} = 2\varepsilon^{2/3} \qquad (10)$$

and C_T^2 is the thermal structure function defined by

$$C_T^2 = \sigma_T^2 = \frac{\langle (\Delta T)^2 \rangle}{r^{2/3}} = 3.2 \chi_T \varepsilon^{1/3} \qquad (11)$$

where

Δu	=	the difference in wind speed
ΔT	=	the difference in the temperatures at two points separated by a distance r
ϵ	=	the dissipation rate of mechanical energy
χ_T	=	the dissipation rate of thermal turbulent energy

Wind-driven turbulence is when $C_V^2 \gg C_T^2$ and temperature-driven turbulence is when $C_T^2 \gg C_V^2$.

2.2 Development of Early Models

Chernov [4] and Tatarski [5] developed the basic model for acoustic single scattering from turbulent eddies in free space. Both assumed the spatial correlation function for the acoustic index of refraction to be a Gaussian function. The theory assumes forward scattering in a homogeneous atmosphere with isotropic turbulence. Both Chernov and Tatarski start with the acoustic wave equation.

$$\nabla^2 p - \frac{(1+\mu)^2}{c_o^2} \frac{\partial^2 p}{\partial t^2} = 0 \qquad (12)$$

where μ is the fluctuating part of the acoustic index of refraction of the medium with $|\mu| \ll 1$. The solution for a single frequency plane wave can be written in the form

9

$$p = A(r) \, e^{-i[\omega t - S(r)]} \tag{13}$$

where

S(r)   =   the phase of the perturbed wave
ω   =   the angular frequency
t   =   time
A(r)   =   the amplitude at distance r.

The Rytov method is used to solve the wave equation. A procedure must be developed to solve for S(r) and A(r) because they are unknown functions. Rytov's method consists of substituting another function:

$$p = A_o \, e^{-i[\omega t - \psi(r)]} \tag{14}$$

into equation (13) and solving for ψ. The resulting relationship for function ψ is

$$\psi(r) = S(r) + i \ln\left(\frac{A(r)}{A_o}\right). \tag{15}$$

In order to simplify the derivation, χ is typically used to represent the $\ln(A(r)/A_o)$. Substituting ψ for p in equation (12), Chernov and Tatarski arrive at the phase and log-amplitude variances, $\langle S^2 \rangle$ and $\langle \chi^2 \rangle$, respectively, assuming a Gaussian correlation function:

$$\langle \chi^2 \rangle = \frac{\sqrt{\pi}}{2} \langle \mu^2 \rangle \, k^2 \, R \, L \left(1 - \frac{1}{D}\tan^{-1}(D)\right) \tag{16}$$

and

$$\langle S^2 \rangle = \frac{\sqrt{\pi}}{2} \langle \mu^2 \rangle \, k^2 \, R \, L \left(1 + \frac{1}{D}\tan^{-1}(D)\right) \tag{17}$$

10

where

D = the wave parameter = $4R/(kL^2)$
L = the scale of turbulence
R = the propagation distance
k = the acoustic wavenumber
$<\mu^2>$ = the variance of the index of refraction fluctuations

The only restriction for this solution is that the phase change and relative change of amplitude must be small between points separated by a wavelength. This condition does not impose any limitations upon the total variation in these quantities.

Chernov and Tatarski examine the two limiting cases. The first limiting case is $D \ll 1$ or $R \ll 0.25 \, kL^2 = R_{cr}$. At 62.5 Hz and greater, turbules with sizes on the order of two times the square root of the range or larger would obey this condition. Applying the limiting condition to equations (16) and (17), yields

$$\langle \chi^2 \rangle = \frac{8\sqrt{\pi}}{3} \langle \mu^2 \rangle \left(\frac{R}{L}\right)^3 \tag{18}$$

and

$$\langle S^2 \rangle = \sqrt{\pi} \langle \mu^2 \rangle \, k^2 \, R \, L. \tag{19}$$

For turbules the size of the propagation path ($R \approx L$), the log-amplitude variance $<\chi^2>$ is on the order of $\langle \mu^2 \rangle$, which is about 10^{-6} for the atmosphere (equations (18) and (19)).

In the opposite case, where $D \gg 1$ or $R \gg R_{cr}$, the quantity $(1/D)\tan^{-1}(D) \ll 1$ and

$$\langle \chi^2 \rangle = \langle S^2 \rangle = \frac{\sqrt{\pi}}{2} \langle \mu^2 \rangle \, k_o^2 \, R \, L. \tag{20}$$

The condition would apply for turbules sizes on the order of one-fourth times the square root of the range or less at frequencies less than 4000 Hz. The solution would be applicable for turbules smaller than 2.5 m at a range of 100 m.

Chernov calculates the transverse autocorrelation function for the phase and amplitude fluctuations. Suppose two receivers lie in a plane located a distance R from a source and are separated by a distance ρ (figure 2). For small values of D (D $\ll$ 1), the amplitude R_χ and phase R_S autocorrelation coefficients are [8]

$$R_\chi = \left[1 - 2\left(\frac{\rho}{L}\right)^2 - \frac{1}{2}\left(\frac{\rho}{L}\right)^4\right]e^{-\rho^2/L^2} \qquad (21)$$

and

$$R_S = e^{-\rho^2/L^2}. \qquad (22)$$

The phase autocorrelation coefficient R_S has a Gaussian shape, which is the same form as the correlation coefficient for the refractive index fluctuations. The amplitude autocorrelation R_χ is not Gaussian.
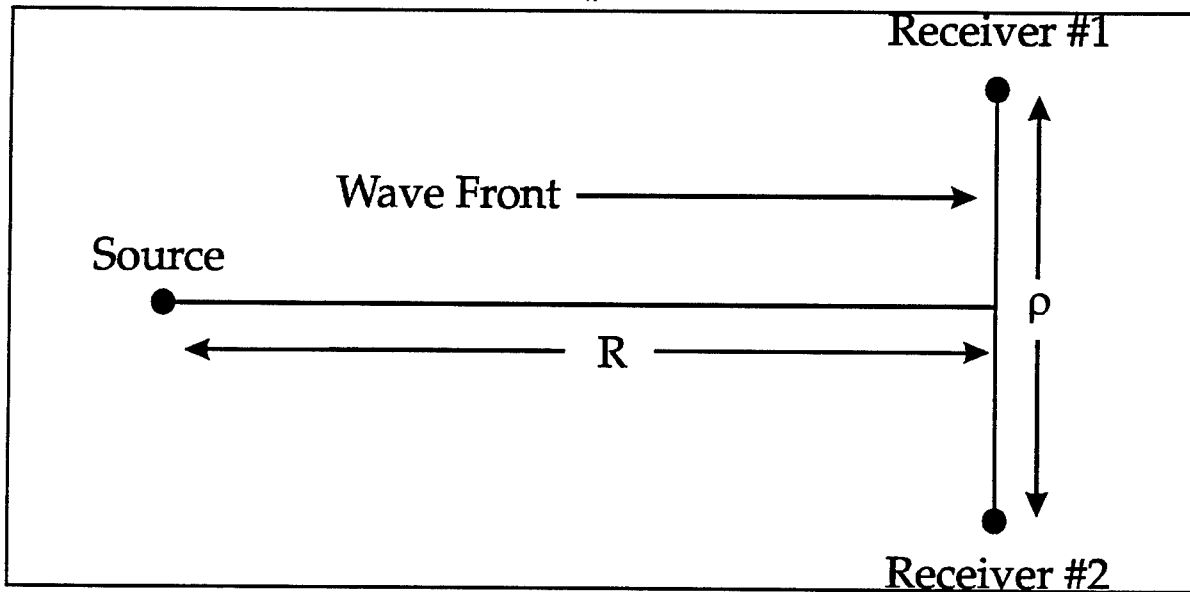
Figure 2. Chernov's geometry.

The corresponding structure functions can be derived once the forms for the phase and log-amplitude variances are known. The structure functions for the log-amplitude $\chi = \ln(p/p_o)$ and phase $S = \phi - \phi_o$ in a plane perpendicular to the direction of propagation are defined as:

$$D_\chi(r,\rho) = \left\langle \left[\chi(\vec{r}+\vec{\rho}) - \chi(\vec{r})\right]^2 \right\rangle \tag{23}$$

and

$$D_S(r,\rho) = \left\langle \left[S(\vec{r}+\vec{\rho}) - S(\vec{r})\right]^2 \right\rangle \tag{24}$$

where r is the distance from the source to the plane and ρ is the transverse separation.

The following relationships hold for the log-amplitude and phase structure functions:

$$D_\chi(r,\rho) = 2\left[\left\langle \chi^2 \right\rangle - B_\chi(\rho)\right] \tag{25}$$

and

$$D_S(r,\rho) = 2\left[\left\langle S^2 \right\rangle - B_S(\rho)\right] \tag{26}$$

because the difference in phase S has a zero mean and the mean of χ is very close to zero for small fluctuations. $B_\chi(\rho)$ and $B_S(\rho)$ in equations (25) and (26) are the transverse correlation function of the log-amplitude and phase fluctuations, respectively.

Starting with the plane wave model used by Tatarski and Chernov, Karavainikov [6] developed a spherical wave model for calculating the log-amplitude and phase variances. When $R/kL^2 \gg 1$, the variance equations have the form

$$\left\langle \chi^2 \right\rangle = \frac{\sqrt{\pi}}{2} \left\langle \mu^2 \right\rangle k^2 L R \tag{27}$$

and

$$\langle S^2 \rangle = \frac{\sqrt{\pi}}{2} \langle \mu^2 \rangle k^2 L \, R. \tag{28}$$

Karavainikov also succeeded in deriving an expression for the phase and log-amplitude transverse correlation functions for the above conditions:

$$B_\chi(\rho) = \langle \chi^2 \rangle \frac{\Phi(\rho/L)}{\rho/L} \tag{29}$$

and

$$B_S(\rho) = \langle S^2 \rangle \frac{\Phi(\rho/L)}{\rho/L} \tag{30}$$

where

$$\Phi(\rho/L) = \int_0^{\rho/L} e^{-u^2} du. \tag{31}$$

Substituting equations (29) and (30) into equations (25) and (26), respectively, gives the log-amplitude and phase structure functions

$$D_\chi = D_S = \sqrt{\pi} \langle \mu^2 \rangle k_o^2 R L \left[1 - \frac{\Phi(\rho/L)}{\rho/L} \right]. \tag{32}$$

The log-amplitude and phase variance equations, equations (27) and (28), provide an estimate of the variance of the acoustic signal caused by small-scale turbulence. These equations have been compared to experimental data over short ranges (R < 500 m). Comparisons [9,10] using equation (32) for L ≈ 1 m showed good results for frequencies of 125 Hz and above. However, the theory severely underpredicts the data at frequencies below 125 Hz. It is not exactly known why the theory underpredicts the effects at low frequencies.

A possible explanation for the model underpredicting the data at frequencies below 125 Hz is contamination of the data by wind noise. [9] Figure 3 shows a comparison between data and predictions of the phase and log-amplitude structure functions for a given signal-to-noise ratio. It happens when the

14

signal-to-noise ratio drops too low, then the background and wind noise are the main sources of acoustic energy causing an overestimate in the data. Wind noise occurs as small-scale turbules, tens of centimeters to tens of meters, move across the microphones resulting in variations in the pressure exerted against the microphone diaphragm. This is a very probable explanation for equation (32) underpredicting the levels below 125 Hz because wind noise is a low-frequency phenomena with its greatest effect below 125 Hz.
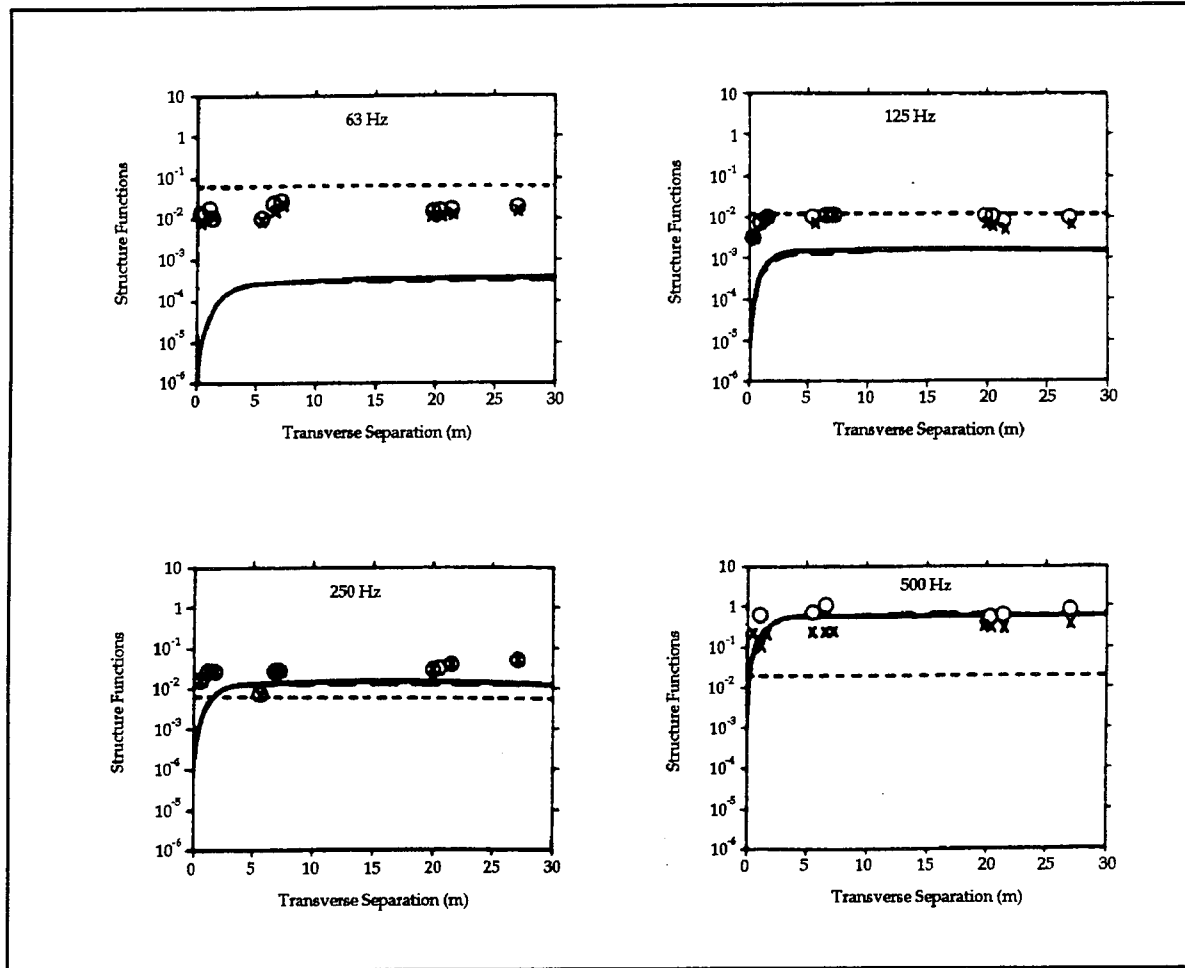
Figure 3. **Comparison of data (o, phase, and x, log amplitude) structure functions with numerical predictions (-, phase and ---, log amplitude) for a source 0.30 m off the ground. The dashed horizontal line represents the particular background noise structure function for each frequency.**

15

The log-amplitude and phase structure functions are related to the coherence function. If the variance in the acoustic signal results mainly from wind noise, then a loss of coherence would be expected. The loss of coherence between two microphones means that the variations occurring at one microphone are not related to the variations occurring at the other microphone. This causes total loss in phase relation between the two microphones resulting in not being able to track an acoustic source.

2.3 Development of New Models

The early turbulence models provided an easy way of estimating the variance of an acoustic signal. However, the early models were, for the most part, a very simplified view of the environment. The environment that sound propagates through includes refraction, diffraction, and complex ground impedance. None of these effects are included in the early models. A researcher must first try to understand what type of small-scale turbulence is present in the atmosphere, including the dynamics of the small-scale turbulence, when developing new models. Current research has focused on the incorporation of scattering models into an acoustic propagation code to gain a better understanding of the physical reality of acoustic scattering by small-scale turbulence. Some of these models will be discussed. The name of the models are not found listed as such in literature. The naming convention of the models in this report is done mainly to associate the model with the person who developed it because names have never really been assigned to the models in the literature.

2.3.1 Daigle Model

The Daigle model could have been named the Karavainikov model because the work and formulas used by Daigle et al. is based on the work done by Karavainikov, [6] Chernov, [4] and Tatarski. [5] The main reason for placing the Daigle model in the new model section is that Daigle et al. took this early work and applied it to a series of experiments conducted during a variety of conditions over relatively short paths (horizontal ranges < 200 m).

Daigle et al. used two Wallac thermoanemometers to measure the temperature and wind velocity as well as the fluctuations. This instrument provided them with a response time of 0.03 s for measuring the fluctuations. Figures 4 and 5 show sample time series of the temperature and wind speed. To obtain turbulence parameters, the autocorrelation of each of the time series were calculated. To maintain a parallel with Karavainikov's work, a Gaussian form was chosen for the spatial correlation function

$$\langle \mu_1 \mu_2 \rangle = \langle \mu^2 \rangle e^{-\xi^2/L^2} \tag{33}$$

where L is a measure of the scale of the turbulence. Using this result, equation (7) can be substituted into this equation resulting in

$$\langle \mu_1 \mu_2 \rangle = \left(\frac{\sigma_v \cos\theta}{c_o} \right)^2 e^{-\xi^2/L_v^2} + \left(\frac{\sigma_T}{2\langle T \rangle} \right)^2 e^{-\xi^2/L_T^2} \tag{34}$$

where
  L_v = the correlation length of the wind
  L_T = the correlation length of the temperature

It can be seen from equation (34) that the spatial correlation function is weighted according to the values of L_v and L_T. The correlation lengths of the wind and temperature were calculated from the autocorrelation of the wind and temperature time series by taking the $e^{-1/4}$ point on the curve, giving the correlation time for the data. The correlation lengths were calculated using Taylor's Frozen Turbulence hypothesis. [11]

From these measurements, Daigle et al. [10] used the results of Karavainikov (equations (27) and (28)) to calculate the log-amplitude and phase variances based on measurement of the turbulence parameters $<\mu^2>$ and L. They also performed experiments to study the transverse and longitudinal relationship of the log-amplitude and phase structure parameter (equation (32)). The results obtained by Daigle et al. were quite good. Most of the turbulence experiments were conducted over regions with relatively low wind speeds and good fetch. This restricted the turbulence effects to mainly thermally driven turbulence.

17
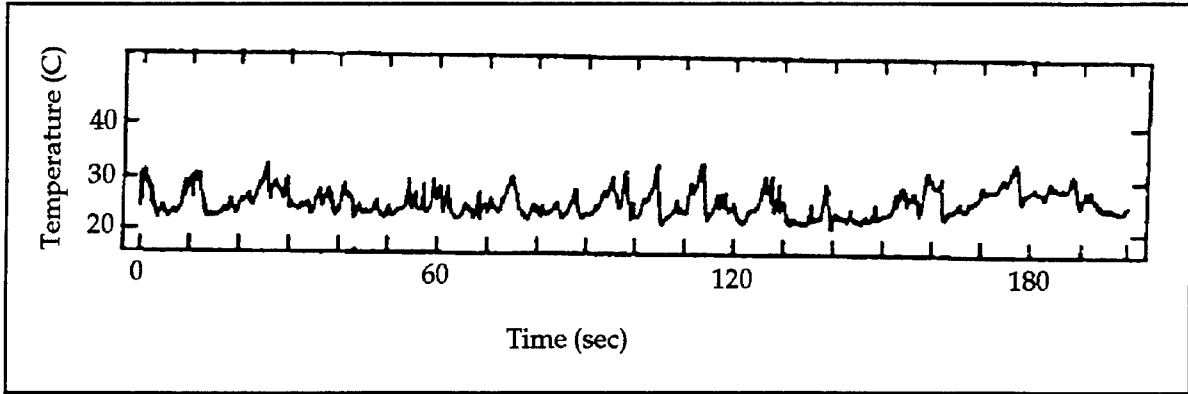
Figure 4. Typical temperature time series showing fluctuations.
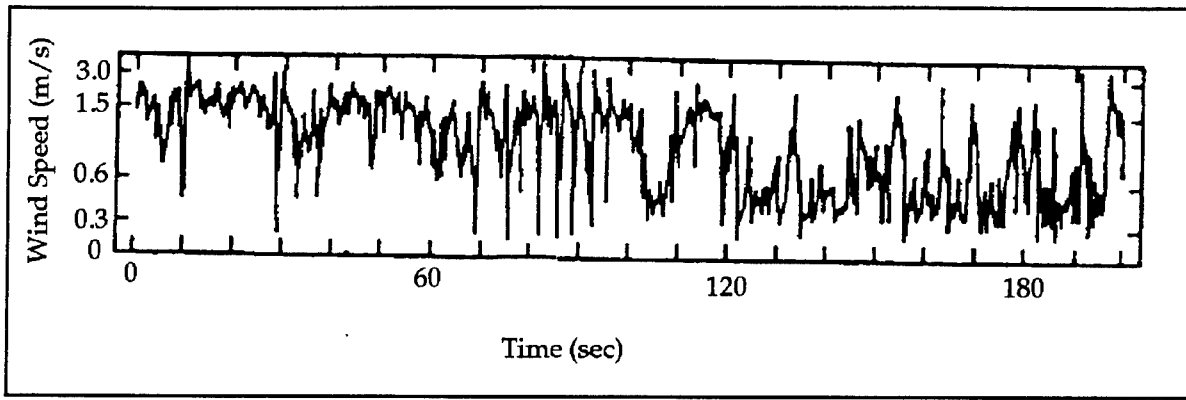
Figure 5. Typical wind speed time series showing fluctuations.

2.3.2   McBride Model

McBride [12,13] developed a computer simulation to model the effect of scattering of acoustic waves by small-scale turbulence in the presence of refraction and complex ground impedance. He developed a scattering equation based on a turbule with a Gaussian index of refraction profile inside it. A first order Born approximation was used to solve the scattering equation. The scattering equation for a given turbule is given by

$$\Psi_i^B = \frac{\sqrt{\pi}}{2} q_i k^2 s^3 \frac{e^{ik(r_{st} + r_{tr})}}{r_{st} r_{tr}} \left(\frac{e^{-Ck^2 s^2/4}}{1 - ia} \right) \tag{35}$$

18

where

$$C = (1 - \cos\Theta)^2 + \frac{\sin^2\Theta}{1 - ia}$$

$$a = \frac{ks^2}{2}\left(\frac{1}{r_{st}} + \frac{1}{r_{tr}}\right)$$

The terms are given by

k = the acoustic wavenumber
r_{st} = the distance from source to turbule center
r_{tr} = the distance from turbule center to receiver
Θ = the scattering angle
s = the size of a turbule
q_i = the value of μ at the center of a turbule

The value used for q_i was derived by work originated by De Wolf. [8] McBride derived a value for q_i using De Wolf's work

$$q_i = \pm\sqrt{\frac{8V\langle\mu^2\rangle}{\pi\sqrt{\pi}NL^3}} \tag{36}$$

where N is the total number of turbules in the volume V and L is the correlation length. The size of the turbule is given by

$$s = \frac{L}{\sqrt{2}}. \tag{37}$$

McBride's model is one of the first models to include the ground effect and the effect of atmospheric refraction on the sound wave. A model run consists of creating a turbulence field and propagating sound waves through it. After the sound has been propagated through the turbulence field, each turbule position is perturbed a small amount and then sound is propagated through the new configuration of turbules. This process is continued until a statistically significant number of iterations are completed. At the completion of each

19

iteration, the complex amplitude of the sound is stored. After all of the iterations have been completed, the variance of the phase and amplitude is calculated along with average phase and amplitude of the received sound field.

McBride's model was compared against the model results and data collected by Daigle et al. (figure 6). Daigle's model consisted of a simple diffraction theory that allowed sound to be diffracted into the refractive shadow zone. The refractive shadow zone is a region where no direct or reflected sound waves can reach the receiver. Diffraction theory works best at the lower frequencies. This can be observed in Daigle's results (figure 6b). The best comparison occurred at 250 Hz. Diffraction theory did not work at all at the higher frequencies. McBride's model compares much better to Daigle's data than the diffraction model did. This seems to indicate that much of the sound at the higher frequencies are due to scattering of turbulence into the shadow zone than by diffraction.
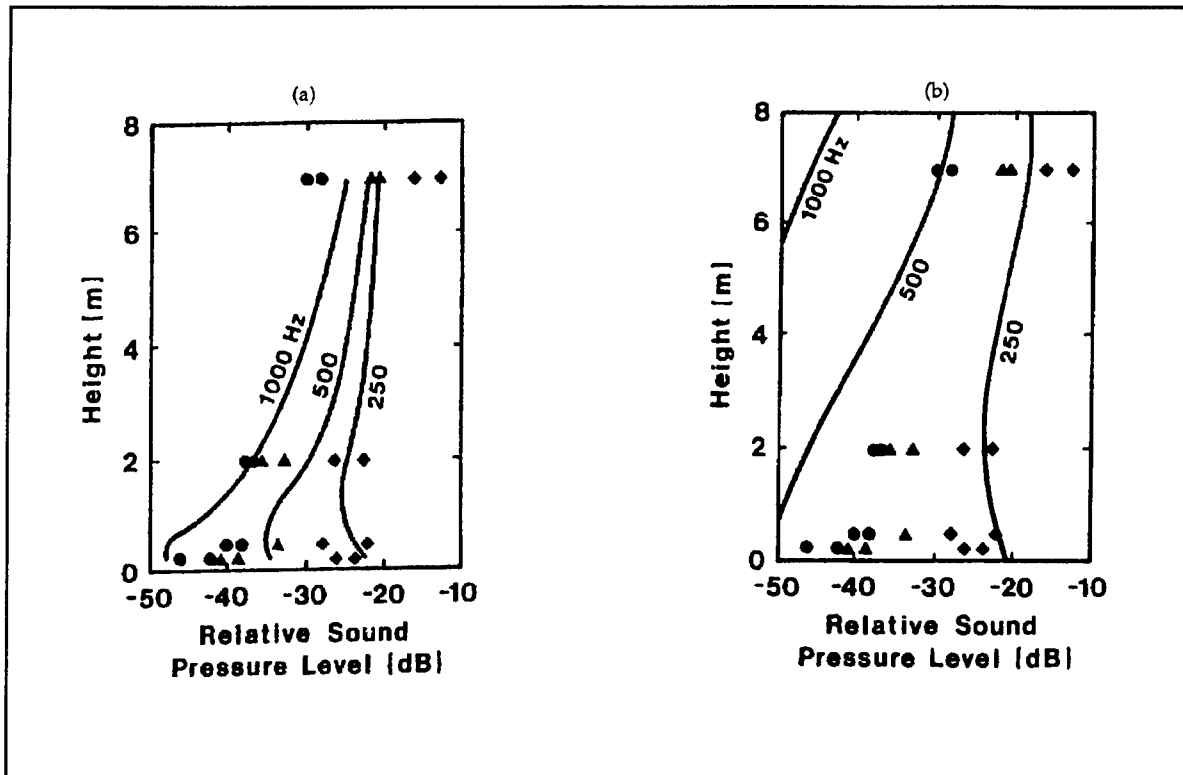
Figure 6. Comparison of measured sound levels (symbols) with predictions based on (a) McBride's turbulence model and (b) diffraction into a refractive shadow zone. Solid circles are 1000 Hz, triangles are 500 Hz, and diamonds are 250 Hz.

2.3.3 Gilbert-Raspet Model

Gilbert et al. [14] integrated a small-scale turbulence model into the Crank-Nicolson Parabolic Equation (PE) to investigate turbulent scattering of sound into a refractive shadow zone. The PE is a good model for the incorporation of turbulence because of the range stepping method of performing calculations, which allows for a two-dimensional cross section of the acoustic field.

To incorporate a turbulence model into the PE, Gilbert et al. had to integrate the turbulence field into the theoretical derivation of the PE. The turbule was incorporated in the acoustic wave equation by rewriting the acoustic index of refraction into a mean value n_d and a fluctuating term μ:

$$n(\vec{R},t) = n_d(\vec{R}) + \mu(\vec{R},t) \tag{38}$$

where

$$
\begin{aligned}
n_d &\simeq 1 \\
\mu &\ll .1 \\
R &= \text{a position vector} \\
t &= \text{time.}
\end{aligned}
$$

Although the fluctuating part is a function of both time and space, the actual calculations adopt the Taylor's frozen turbulence hypothesis [11] and consider propagation of sound for a model with μ evaluated at a particular instant of time.

With this propagation model, Gilbert et al. could perform a two-dimensional propagation of sound through a turbulent field. They concentrated their studies on turbulent scattering into refractive shadow zones over a frequency range of 400 to 800 Hz. They showed a two-dimensional gray-scale plot of the relative sound pressure level for a case of strong upward refraction, which creates a shadow zone region. Next, they ran their turbulence model to create a new gray-scale plot. The new plot showed acoustic energy being scattered into the shadow zone.

A comparison to data taken by Weiner and Keast [15] was made (figures 7 and 8). The result for weak upward refraction shows the model gave good comparison to the data. In the strong upward refraction case, the model either underpredicted or overpredicted the scattering levels.
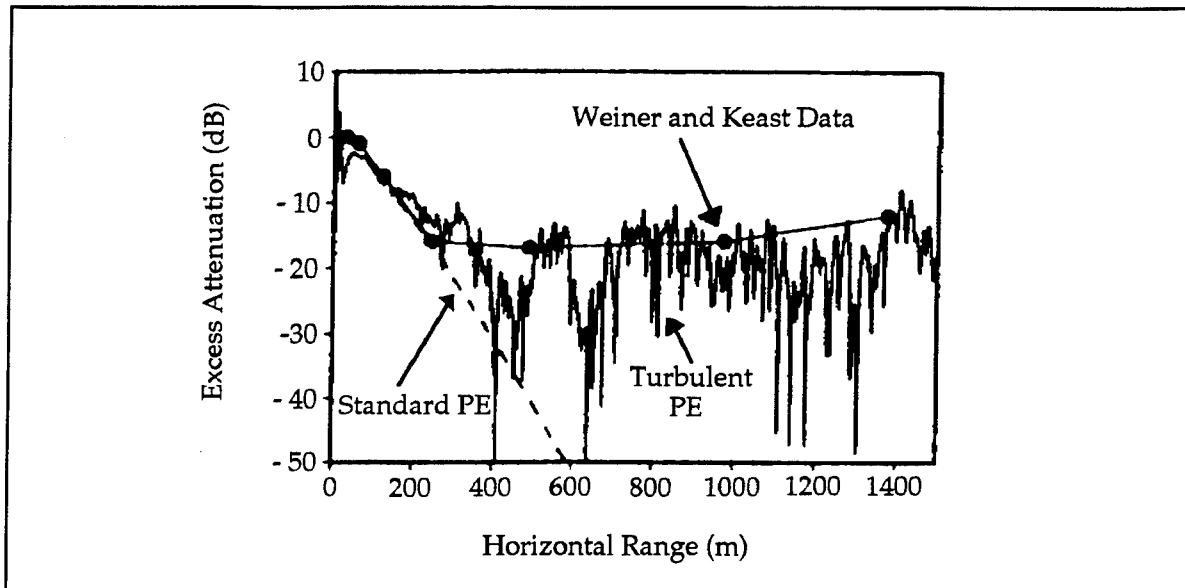
Figure 7. Comparison of Gilbert's turbulent PE model to experimental data and the standard nonturbulent PE for weak turbulence.
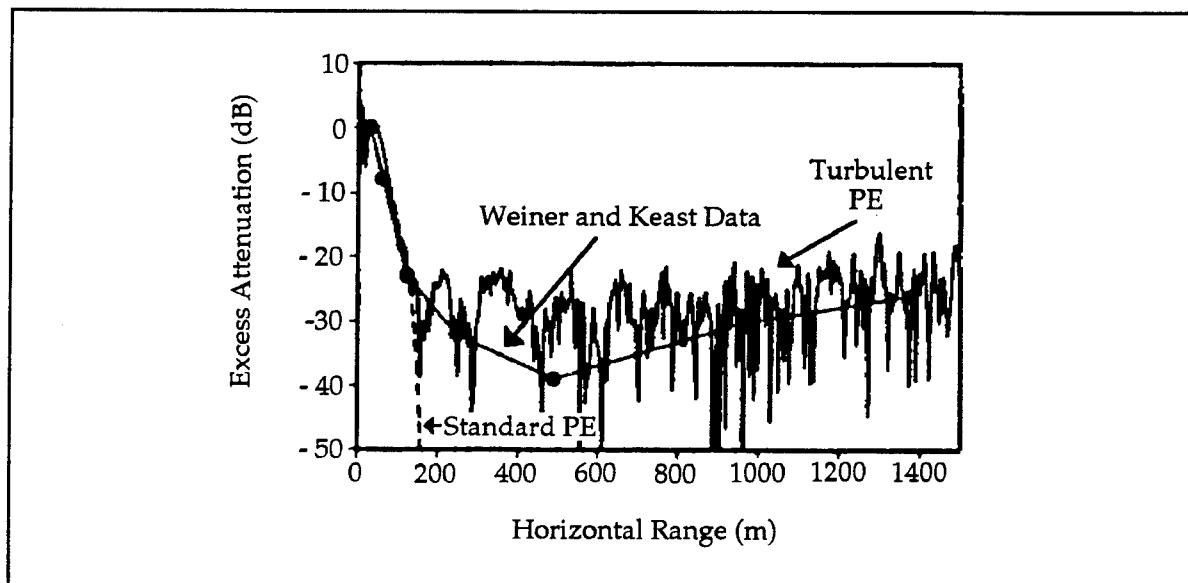
Figure 8. Comparison of Gilbert's turbulent PE model to experimental data and the standard nonturbulent PE for strong turbulence.

2.3.4 Auvermann Model

Auvermann [16,17] is developing a turbulence model to be used in atmospheric acoustic scattering calculations that includes effects not addressed in the statistical model of turbulence. The need for a new model arises from acoustic propagation paths associated with Army operations that are usually dominated by atmospheric conditions near the ground. Turbulence near the ground is not homogeneous nor isotropic, whereas the statistical model assumes these conditions. Additionally, near-ground turbulence inhomogeneity sizes are limited by the upper scale length, whereas the statistical model uses the Kolmogorov spectrum. The size range of the Kolmogorov spectrum is unlimited. The new model pictures the turbulent region as consisting of a collection, or ensemble, of turbules of different sizes with each turbule described by an assumed morphology. A turbule is defined to be a localized inhomogeneity, either temperature or velocity. Thus, this model has been given the name of Turbule Ensemble Model (TEM). TEM has the flexibility needed to show anisotropy using anisotropic turbules and the flexibility to show inhomogeneity using variable concentrations of turbules of different sizes. Finally, an upper-scale limit can be imposed on TEM by cutting off the concentration distribution at the appropriate size. A description of the scattering properties of a velocity turbule ensemble will follow. A similar discussion can be made for temperature turbules.

The first step in determining the scattering properties of a velocity turbule ensemble is to define mathematically the velocity distribution within a single turbule. The velocity distribution function that has been used is the following:

$$\vec{v}_i(\vec{r}) = \vec{\Omega}_i \times \vec{r} e^{-\vec{r} \cdot \vec{r}/a_i^2} \qquad (39)$$

where

$\vec{\Omega}_i$ = an angular velocity vector

$\vec{r}$ = the vector position of a field point within the turbule

a_i = the characteristic size of the turbule

and the exponential localizes the velocity distribution to the turbule.

23

The angular velocity vector within the turbule can be derived in terms of the characteristic size of the turbule. The maximum velocity occurs at a radial distance in the meridian plane of $a_i / 2^{1/2}$. It can be shown [5] that turbule velocity scales as turbule size is raised to the two-thirds power using dimensional arguments. Specifying index one to be the largest turbule to be considered and its velocity maximum to be v_1, then the magnitude of the angular velocity vector within the turbule can be written

$$\Omega_i = \sqrt{2e}\left(\frac{v_1}{a_1^{2/3}}\right) a_i^{-1/3}. \tag{40}$$

According to the relationship, the angular velocity of the smaller turbules is larger than the larger turbules.

The acoustic scattering cross section of a turbule with the velocity distribution of equation (39) has been derived using the Born approximation. The derivation started with a wave equation deduced by linearizing the Navier-Stokes equation in the acoustic variables, at the same time retaining the velocity inhomogeneity to first and second order in the small quantity v_i / c_∞ as a source term. The incident wave was substituted for the internal wave in the turbule to arrive at the following expression for the first order scattering efficiency $Q_i^{(1)}$

$$Q_i^{(1)}(k\hat{r}) = (\Omega_i a_i/4c_\infty)^2 (ka_i)^6 \sin^2\theta \, \cos^2\theta \, \sin^2\theta_\alpha \, \sin^2(\phi - \phi_\alpha)$$
$$\exp[-(ka_i)^2(1 - \cos\theta)] \tag{41}$$
$$k = 2\pi/\lambda$$
$$Q_i^{(1)} = \sigma_i^{(1)}/\pi a_i^2$$

where

(θ, ϕ) =   the polar and azimuthal angles of the unit vector $\hat{r}$ directed toward the observation point

$(\theta_\alpha, \phi_\alpha)$ =   the polar and azimuthal angles of the angular velocity vector $\vec{\Omega}_i$

$\sigma_i^{(1)}$ =   the scattering cross section.

It is necessary to add up the scattering caused by all turbules in the scattering volume to calculate the scattering to be expected in an experiment or in some battlefield scenario. A self-consistent field method [18] from solid state theory is used to sum the scatter from a turbulent field. The notation used in the summation is

$$\left| \pi_T(\vec{r}) \right\rangle = \left| p_i \right\rangle + \sum_j \hat{T}(\vec{r};\vec{r}';\vec{b}_j) \left| \pi^j(\vec{r}') \right\rangle$$

$$\left| \pi^j(\vec{r}') \right\rangle = \left| p_i \right\rangle + \sum_{m \ne j} \hat{T}(\vec{r}';\vec{r}'';\vec{b}_m) \left| \pi^m(\vec{r}'') \right\rangle$$

(42)

where

π_T	=	the total field at the observation point
p_i	=	the incident field
π^j (or π^m)	=	the self-consistent field at the scatterer location
$\hat{T}$	=	the integral operator representing the scattering properties of the scatterer located at position $(\vec{b}_j, \vec{b}_m)$.

The turbulent scattering model must be combined with an acoustic propagation model in order to account for nonturbulent atmospheric conditions such as refraction, diffraction, terrain, and molecular absorption. To include each of these effects, the scattering model is being incorporated in the Fast Field Program (FFP). The FFP is a one-way full wave acoustic propagation model developed 10 years ago for atmospheric acoustics. [19,20] FFP admits only one source, which is considered isotropic, (i.e., one that radiates equally in all directions). As a first step in overcoming these limitations, a new model called the Acoustic Multi-Stream Propagation Program (AMPP) is being developed that uses FFP as a subroutine. There is the problem of scatterers not producing isotropic scattering fields. It is contemplated that approximating anisotropic sources/scatterers as multipoles consisting of particular arrangements of isotropic sources will constitute a solution to the problem.

A general idea of the scattering properties as predicted by the structural approach to turbulence may be had by considering the angular pattern of a single turbule as given in equation (41). This has rather striking dependence

on the observation direction and on the turbule spin axis orientation. It goes to zero if $\theta_\alpha = 0$ or π; $\phi = \phi_\alpha$ or $\phi_\alpha \pm \pi$; or $\theta = 0$, $\pi/2$, π. For example, suppose that $\theta_\alpha = \pi/2$, $\phi_\alpha = 0$. Then the scattering is zero at $\phi = (0, \pi)$ and $\theta = (0, \pi/2, \pi)$, and has maxima at $\phi = (\pi/2, 3\pi/2)$ and $\theta = (\pi/4, 3\pi/4)$. For ka > 1, the exponential becomes important, and strongly reduces scattering in the backward hemisphere relative to the forward.

This differential efficiency also has an unusual dependence on ka and goes as $(ka)^6$. This is quite different from Rayleigh scattering, which goes as $(ka)^4$ with a very different dependence on the scattering angle.

It is of great interest to consider the efficiency averaged over random orientations of the spin axis. This gives

$$\langle Q_i^{(1)}(k\hat{r}) \rangle = (1/3)(\Omega_i a_i/4c_\infty)^2 (ka_i)^6 \sin^2\theta \cos^2\theta$$
$$\exp[-(ka_i)^2(1 - \cos\theta)] . \tag{43}$$

This averaged scattering efficiency is plotted versus θ for two values of ka in figure 9 for $(\Omega_i a_i /4c_\infty) = 0.1$. The characteristic scattering peaks at 45° and at 135° are readily apparent, creating the appearance of a multipole field. The vanishing cross section results in the forward direction contrasts with the result Tatarski's formula, which grows without bound in the forward direction. This disparity results from the use of the unlimited size spectrum of Kolmogorov in the formula of Tatarski.

It is interesting to consider the Optical Theorem in connection with the cross section formula of equation (41). The Optical Theorem states that the total scattering cross section is equal to the imaginary part of the scattering amplitude in the forward direction. The cross section is obtained by multiplying the scattering amplitude by its complex conjugate. In the Born approximation result above, the scattering cross section in the forward direction is zero, so the imaginary (and the real) part of the scattering amplitude must be zero. This is a contradiction because the total cross section is non-zero. This contradiction is resolved in the second Born approximation. The second Born forward imaginary scattering amplitude is identically equal to the first

Born total scattering cross section, indicating that the Optical Theorem is true for these approximate formulas, but in a rather novel way.
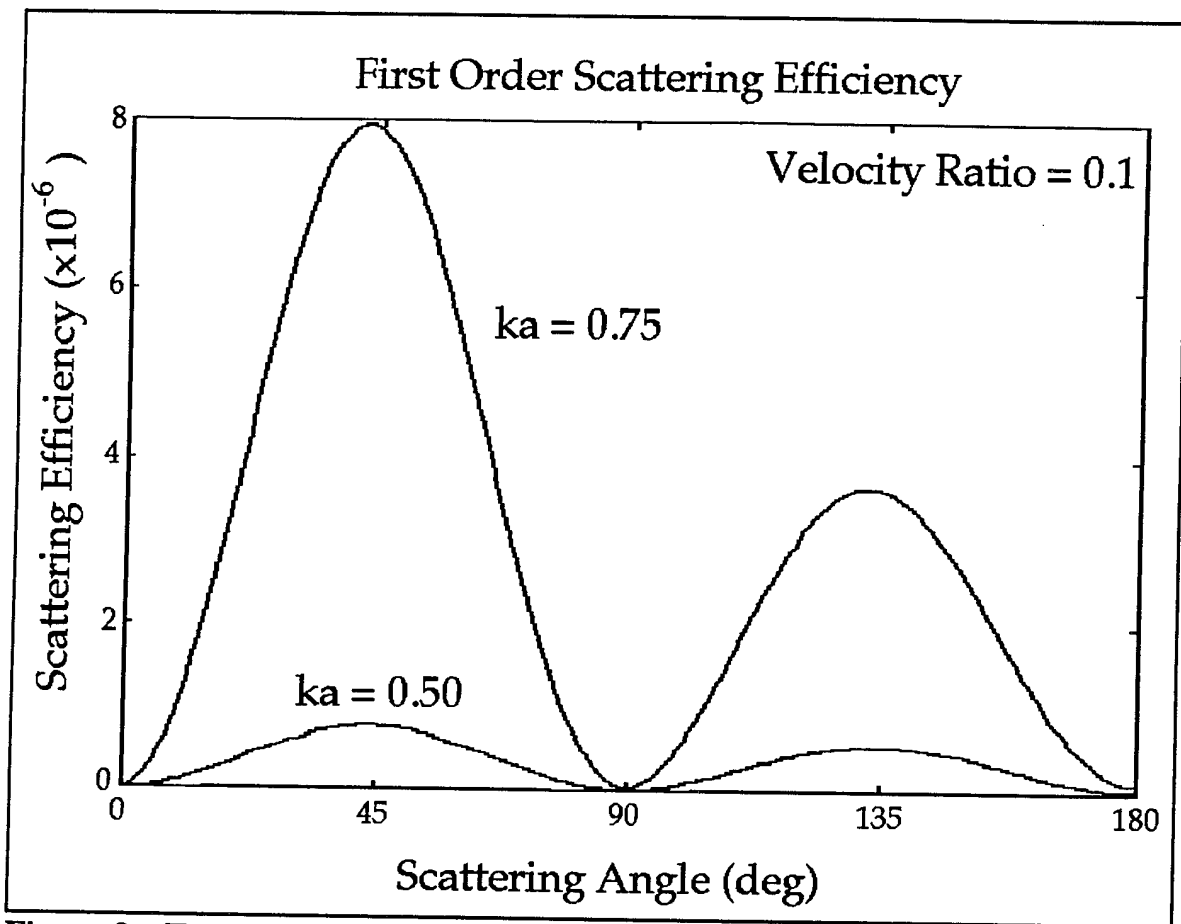
Figure 9. Turbule acoustic scattering efficiency.

3. Large-Scale Turbulence

Some work through the years has dealt with the effect of large-scale turbulence on propagation. Unfortunately, large-scale turbulence is difficult for meteorologists to characterize. The net result is that there are no good ways of modeling the large-scale turbulence. Measurements are also difficult because of the dimensions of the turbulence being on the order of hundreds of meters to kilometers in height and length. In recent years, some simple models for large-scale turbulence have been derived. Measurements can now be made of the large-scale turbulence with the new remote profilers. Better models can be derived with these measurements.

3.1 Characteristics of the Planetary Boundary Layer

It is convenient to consider the atmosphere to be divided into a number of horizontal layers when discussing the details of air flow (figure 10). The region in which the atmosphere experiences surface effects through vertical exchange of momentum, heat, and moisture is called the planetary boundary layer (PBL) or sometimes referred to as the friction layer. The PBL is the region where the atmosphere experiences surface effects through vertical exchange of momentum, heat, and moisture. The vertical extent of the PBL is quite variable. Panofsky and Dutton [2] define the depth of the PBL, h, as the thickness of the turbulent region next to the ground, which is also called the depth of the mixed layer or the mixing layer. Another height used to describe the thickness of the PBL in the daytime is the height z_i of the lowest inversion. Actually, h tends to be 10 percent or so larger than z_i because the lowest part of the inversion is still turbulent, partly because of overshooting from below, and partly because there is often strong wind shear in the inversion. Therefore, the height of the lowest inversion is a good approximation of the thickness of the PBL during the daytime.

The lowest part of the PBL is called the surface layer. The characteristics of turbulence and the vertical distribution of mean variables are relatively simple in the surface layer. There is no precise definition of the surface layer. Qualitatively, the surface layer is that part of the PBL immediately above the surface, where vertical variations of vertical fluxes can be ignored. Typically,
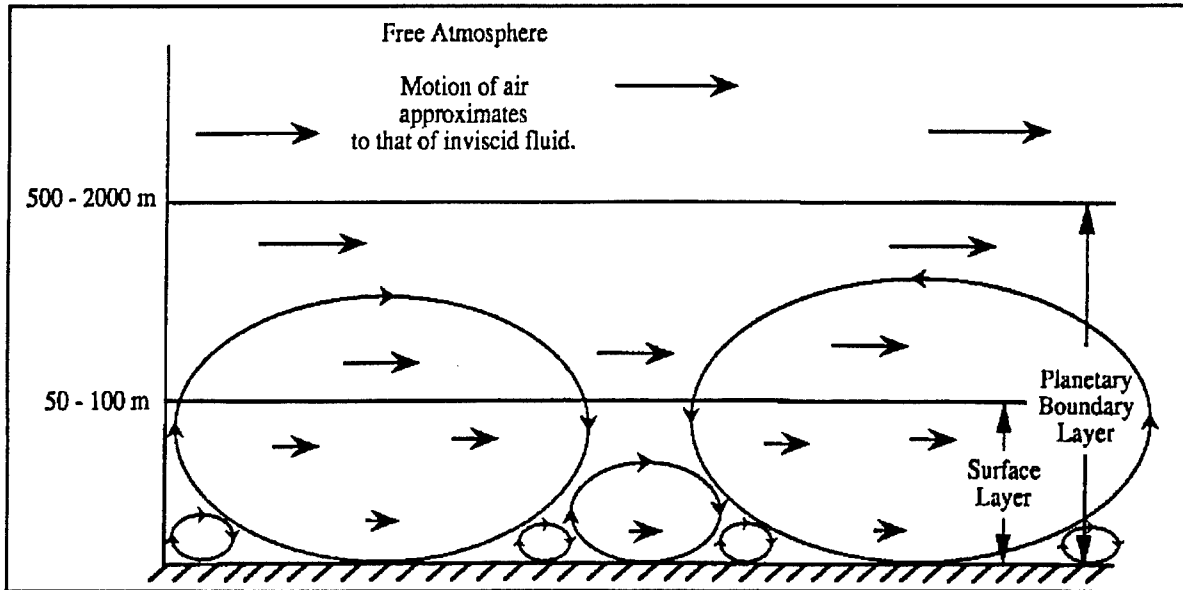
Figure 10. Breakdown of the lower atmosphere.

the fluxes are large at the surface and decrease to zero near the top of the PBL. If the decrease of flux with height is linear, then fluxes decrease by a factor of 10 percent in the lowest 10 percent of the PBL.

A rational method must be found to superimpose the effects of both mechanical and thermal forcing. These two types of forcing influence the turbulence and the variation of the mean variables even in the surface layer. The method to combine the two types of forces was first accomplished by Monin and Obukhov through their similarity theory. They introduced two scaling parameters, essentially independent of height in the surface layer, for velocity and length. These are the friction velocity u_* and the Monin-Obukhov length L_{mo}.

The question is how to determine the Monin-Obukhov length, the friction velocity, and the inversion layer thickness. The quantity L_{mo} depends primarily on vertical heat flux at the surface and the friction velocity. There are two ways to obtain values for L_{mo}. Pasquill [21] provides the following equation to calculate the value of L_{mo}:

30

$$L_{mo} = -\frac{u_*^3 c_p \rho T}{k g H} \tag{44}$$

where

k	=	the von Karman constant = 0.4
g	=	gravitational acceleration
H	=	the vertical heat flux density
T	=	temperature
ρ	=	the density of air
C_p	=	the specific heat at constant pressure

Typically, equation (44) is not easy to work with. Another way used by the acoustic community for obtaining L_{mo} is to estimate it from the Turner classes, which were developed for use in air pollution studies. The Turner classes range from 1 to 7, with 1 for strong convection, light-wind conditions, 4 for purely mechanical turbulence, and 7 for stable stratification. The Turner class is determined from the wind velocity and an estimate of solar radiation using table 1. Because L_{mo} is also a function of surface roughness, this parameter must also be included in estimating L_{mo} from the Turner class. Table 2 shows the estimates of L_{mo} given Turner classes for the case where the roughness length is 0.05 m.

Table 1. Estimation of Turner classes (daytime only)

Surface Wind Speed at 10 m (m/s)	Incoming Solar Radiation		
	Strong	Moderate	Light
<2	1	1	1
2-3	1-2	2	3
3-5	2	2-3	3
5-6	3	3-4	4
> 6	3	4	4

Table 2. Estimation of L_{mo} for various Turner classes

Turner Class	$-L_{mo}$
1	8-12 m
2	12-20 m
3	20-60 m
4	>60 m

The friction velocity is defined as:

$$u_* = \sqrt{\frac{\tau}{\rho}} \tag{45}$$

where τ is the Reynolds stress tensor and ρ is the density of air. The value of the friction velocity depends on the wind speed and roughness length. It is used to normalize various turbulence statistics. This allows comparison of turbulence statistics between atmospheric conditions with differing wind velocity. If variations in u are due to purely mechanical turbulence, an alternate empirical formula for u_* can be used for $z > z_o$:

$$u_* = \frac{uk}{\ln(z/z_o)} \tag{46}$$

where

k	=	the von Karman constant
z	=	the height
u	=	the wind speed at height z
z_o	=	the roughness length

For the case of purely mechanical turbulence, the friction velocity can be calculated given a wind speed at a height over an area with a particular roughness length. Table 3 provides typical values for roughness lengths. [2]

32

Table 3. Typical roughness lengths

Ground Cover	Roughness Length (m)
Water or Ice	10^{-4}
Mown Grass	10^{-2}
Long Grass, Rocky Ground	0.05
Pasture Land	0.2
Suburban Housing	0.6
Forests, Cities	1-5

The main problem is calculating the lowest inversion z_i. This value is important because it represents the largest size an inhomogeneity can be in the atmosphere. According to Panofsky and Dutton, the horizonal wind speed fluctuations are related to z_i by

$$\frac{\sigma_u}{u_*} = \left(12 - 0.5\frac{z_i}{L_{mo}}\right)^{1/3}.$$ (47)

Substituting equation (46) into equation (47) and solving for z_i results in

$$z_i = 2L_{mo}\left[12 - \left(\frac{\sigma_u}{ku}\right)^3 \ln^3(z/z_o)\right].$$ (48)

Equation (48) provides the height of the lowest inversion in terms of Monin-Obukhov length, the fluctuation of the horizontal wind speed, and the roughness length. This result will be useful in determining the upper limit to the size of large-scale turbulence during the daytime.

3.2 Experimental Evidence of Large-Scale Turbulence

Some of the early experiments that indicate large-scale inhomogeneities were conducted by Rudnick. [22] The experiment was conducted in an anechoic chamber introducing temperature inhomogeneities by heating a 5-m-long resistance wire stretched across the room to control the environmental

parameters. Rudnick was only investigating the effects of temperature driven turbulence on acoustic propagation. Rudnick scaled the frequencies from 4 to 6 kHz because the experiment was conducted in an anechoic chamber. The scaling of frequencies must be done so the results of the experiment will scale correctly when applied to the atmosphere. Rudnick's results showed that two temporal scales were present, a short- and long-term fluctuation.

Ingard, [23] in his review of meteorological effects on acoustics, presented several graphs of sound pressure levels recorded on a windy day. The variation in the sound pressure levels were about 15 to 20 dB at 2 kHz for wind speed varying between 6 and 11 m/s. Ingard uses the term gusty to refer to these variations in the wind speed. According to Ingard, the average attenuation due to the gustiness of the wind is about 4 to 6 dB/100 m with fluctuations sometimes going as high as 20 dB. He also states that anemometer records show that the average size of the turbules often lie in a region of 2 to 8 m in diameter with much larger turbules also occurring, even up to 1000 m.

Wiener and Keast [15] performed several experiments of outdoor sound propagation. They used bands of random noise for their experiments. The wind speed and direction were measured at a height of 10 ft and the pressure, wet- and dry-bulb temperatures at 6 ft. A typical sampling time for the acoustical and meteorological data was 30 s. At the 200-ft range, the peak-to-peak fluctuations were 12 dB for a band of noise centered at 425 Hz and 25 dB for a band of noise centered at 850 Hz. These measurements were for a receiver situated upwind of the source.

Chessell [24] used the theoretical relations of Chernov and his own measurements to determine the scales of atmospheric turbulence that have the greatest effect on acoustic signals. Chessell chose a different approach to measure the fluctuations. The source for the experiment was a series of surface firings of small charges of TNT located at two positions at ranges of 4.3 and 9.3 km and at angles of 90° and 70°, respectively, to a linear array of five microphones with uniform spacing of 100 m. A sixth microphone was located 600 m to the side and 300 m ahead of the uniform array.

34

Wind and temperature profiles were measured to a height of 3 km at the start of each observational period using conventional radiosondes and theodolite tracking. Continuous observations of surface temperature, wind speed, and direction were also made at a position near the first microphone in the linear array. Each observational series consisted of 30 firings spaced 1-min apart.

Chessell then calculated the ratio of the correlated to uncorrelated standard deviations given by

$$\frac{\sigma_{\Delta t}}{\sqrt{2}\,\sigma_t} = \sqrt{1-\rho} \qquad (49)$$

where

ρ = the spatial correlation coefficient between adjacent paths

$\sigma_{\Delta t}$ = the standard deviation of the time difference fluctuations of the amplitude

σ_t = the standard deviation of the random propagation time fluctuations.

For both the large and the small wave parameter D from Chernov and Tatarski, the ratio rises smoothly to be almost unity when the separation is approximately twice the turbulence scale size. Using these techniques, Chessell determined that turbulence scale sizes have a range of 200 to 500 m with a mean size of 320 m.

A series of line-of-sight propagation measurements where made over a relatively flat open farm land during a period from mid-June 1984 to mid-July 1985. [9] A run consisted of an 8-min record of signals received simultaneously at five transverse microphones mounted 1 m above the ground and one microphone mounted near the source for a reference. The sound source was driven by a tape with a prerecorded signal consisting of a mixture of eight tones centered at one octave spacing beginning at 62.5 Hz.

The Fast-Fourier Transform (FFT) of the measured amplitude and phase contains the spectrum of the fluctuations of the sound field due to turbules present in the atmosphere. The spectral peaks are related to the scale of

turbulence L by Taylor's hypothesis of frozen turbulence, which relates the temporal and spatial turbulence scales by [7]

$$L = \bar{u}\,\tau \tag{50}$$

where $\bar{u}$ is the mean wind speed and τ is the characteristic time associated with the temporal measurements. This hypothesis assumes a slowly changing invariant pattern of turbulence that is convected past the detector with the speed of the mean wind speed.

Taylor's equation can be rewritten as

$$L = \frac{\bar{u}}{\nu} \tag{51}$$

where $\nu = 1/\tau$. Calculations of L show the different scales of turbulence present in the atmosphere during the experiment. Figures 11(a,b) and 12(a,b) show two examples of the phase difference and their FFT. Figures 11a and 11b are for a run where the wind speed is low, a few meters per second. The spectrum (figure 11b) shows several peaks, which represent the different scales of turbulence present in the atmosphere for the run. Figures 12a and 12b are for a run where there was a high wind speed. The only spectral peak present is one at a low frequency. This implies that the only scale of turbulence that is affecting the phase is on the order of a few hundred meters in size.

Some caution must be noted about this type of analysis. The location of the low-frequency peak may be a result of insufficient frequency resolution because of the length of the sample analyzed. A longer time sample might shift the low-frequency peak to a lower frequency suggesting the presence of a larger scale of turbulence.
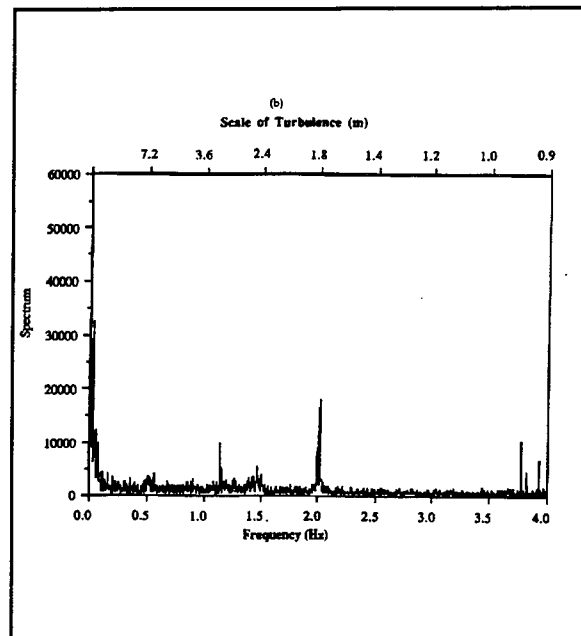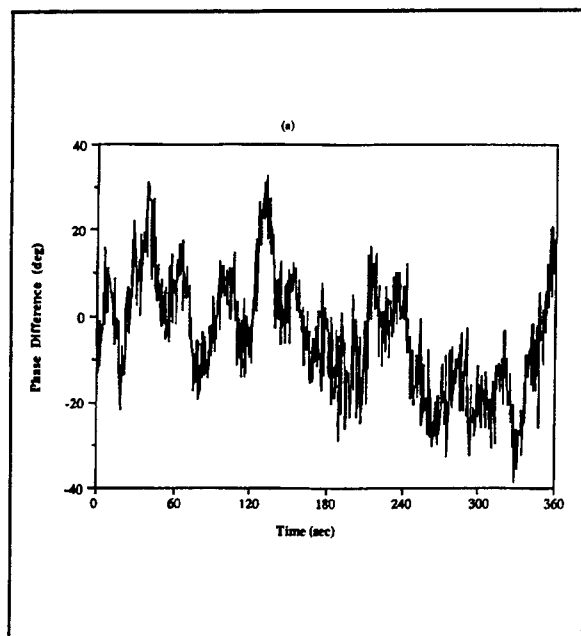
Figure 11. (a) Time series and (b) spectrum of acoustic phase at a microphone for low wind speed.
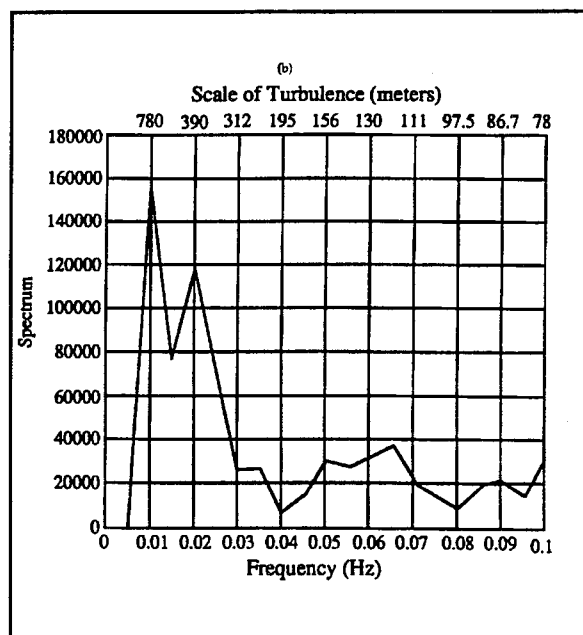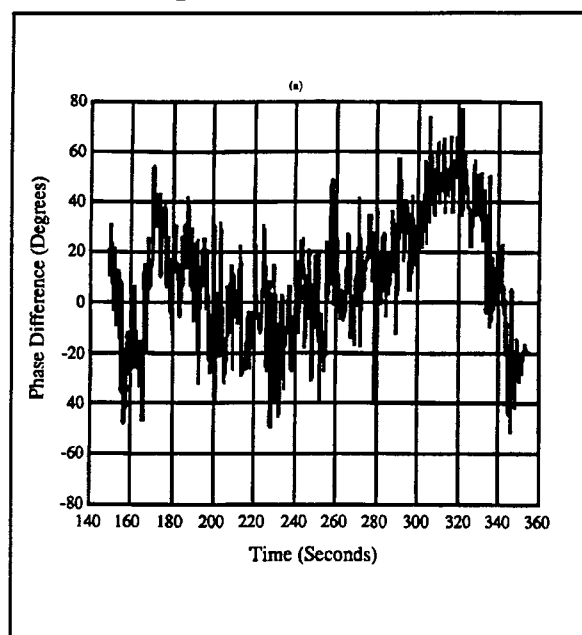
Figure 12. (a) Time series and (b) spectrum of acoustic phase at a microphone for high wind speed.

3.3 Development of Large-Scale Models

The effects from large-scale turbulence through the years have been ignored because of the short time intervals used to take measurements. The lack of observations have lead to very few large-scale turbulence models being developed. Another problem that has lead to a lack of experimental data for large-scale turbulence is the short ranges of most propagation experiments. Until recently, most propagation experiments were over ranges of a few hundred meters. This restriction was mainly because of a lack of reliable sound source capable of producing enough sound to propagate the distances needed for large-scale turbulence studies. Despite these restrictions, a few large-scale turbulence models have been developed. As in section 2, the name of the models are not found listed as such in literature. The naming convention of the models in this report is done mainly to associate the model with the person who developed it because there has never been names assigned to the models in literature.

3.3.1 Chernov/Tatarski Scatter Model

In the derivation of Chernov and Tatarski (section 2.2), the result for the phase and log-amplitude variances equations (18) and (19) was only limited by forward scattering in a homogeneous atmosphere with isotropic turbulence. In the first limiting case where $D \ll 1$, the solution is valid for turbulence up to a few hundreds of meters in size. Turbulence up to a few meters in size can still be considered isotropic turbulence. The resulting equations for the log-amplitude and phase variances in the limit where $D \ll 1$ or $R \ll 0.25 \, kL^2$ are

$$\langle \chi^2 \rangle = \frac{8\sqrt{\pi}}{3} \langle \mu^2 \rangle \left(\frac{R}{L} \right)^3 \tag{52}$$

and

$$\langle S^2 \rangle = \sqrt{\pi} \, \langle \mu^2 \rangle k_o^2 RL. \tag{53}$$

The log-amplitude variance is frequency independent whereas the phase variance is proportional to the square of the wave number (equations (52) and (53)). The log-amplitude variance will remain constant for different

frequencies. An example of expected variances is shown in table 4. The variance of the log-amplitude is very small at small ranges and increases as the cube of the range. The magnitude of the phase variance is much larger than the log-amplitude variance because the phase variance is proportional to the outer scale L.

Table 4. Example of log-amplitude and phase variance of large-scale turbulence (500 m) at 100 Hz with $<\mu^2> = 10^{-6}$

Range (m)	$<\chi^2>$	$<S^2>$
100	3.8×10^{-8}	0.35
1000	3.8×10^{-5}	3.54
10000	3.8×10^{-2}	35.4

However, this model has several limitations. First, this model is derived for free space forward scattering in a homogeneous atmosphere with isotropic turbulence. At large ranges, the scattering from reflected waves will add in as well as scattering from multipath waves. The real atmosphere is not homogeneous, which creates multipaths through refraction and increases the travel distance from the source to receiver. Also, as the size of the turbulence increases, the restriction of isotropic turbulence no longer holds. As the turbulence becomes too large, the dominating effect is due to variations in refraction of the atmospheric profile rather than to scatter.

3.3.2 Roth Thermal Model

Roth [25] developed a model for large-scale effects based on thermal plumes. He used a multipath ray trace routine to calculate the received signal amplitude. Roth concluded that the effects due to temperature fluctuation do not have as great an effect on the fluctuations of the sound speed as wind speed fluctuations. The local sound speed was written as

$$c = c(T) + \vec{u} \cdot \hat{r}. \tag{54}$$

A change in temperature of 2° when the mean temperature is 300 K would cause a change in the sound speed of about 1 m/s (equation (54)). Wind speed fluctuations are greater than 1 m/s on a typical day. As a result, Roth assumes an isothermal atmosphere for his model. Roth calculates the contribution of humidity to the sound speed from

$$c = 20.05\sqrt{T}\left(1 + 0.14\frac{e}{p}\right) \qquad (55)$$

where e is the water vapor partial pressure and p is the atmospheric pressure. Roth concludes that the daily variation of sound speed due to changes in humidity will be less than 1 m/s and short term variation even less. Therefore, he also ignores any effects due to humidity in his model.

Thermals are a basic convectional process formed in the surface layer. The scale of the thermal is known to be of the order of the height of the convective boundary layer. This is equal to z_i, which is the height of the capping inversion. During midday summer conditions, z_i is typically 1 to 1.5 km. Roth assumes that for neutral to unstable conditions, z_i varies from 100 to 2000 m. Assuming the wind speed varies from 2 to 6 m/s, the characteristic time for thermals is 16 s < τ < 17 min. Thermal plumes are apparent in a temperature record as positive pulses. Typically, the pulses are ramp-shaped, a slow rise in temperature followed by an abrupt drop. This can be seen in figure 4 between 165 and 180 s. The important factor about a thermal plume is a sharp rise in the wind speed after the temperature drops back to the previous level (figure 5). It is this sharp rise in the wind speed after the passage of the thermal plume that causes the significant fluctuation in the received acoustic wave.

Roth measured the mean wind speed profile and the standard deviation of the wind speed during an experiment. To create the wind speed profile for his model, he used the measured mean wind speed profile. To simulate the passage of the thermal, he varied the mean wind speed profile by increasing the profile by one standard deviation and decreasing the mean wind speed profile by two standard deviations. The ground impedance model used was not well defined. In the two theoretical cases Roth examined, he predicted variations

in the received relative sound pressure level of about 30 dB at a range of 100 m with source and receiver at a height of 3 m.

3.3.3 Noble Mechanical Model

Noble [26] developed a model for large-scale effects based on a vortex pair of eddies. Noble made the same assumption as Roth, that the temperature and humidity fluctuations have a minor effect on the speed of sound compared to the wind fluctuations. This model is based on results obtained from a series of short range field experiments. It was observed that the phase fluctuations (figure 11a) appeared to have two different time scales from these results. To try and determine which time scales where being observed, a FFT of the phase fluctuations was calculated (figure 11b). A variation on Taylor's hypothesis of frozen turbulence was used to interpret the spectrum. If the assumption is made that turbulence of a certain size causes a unique temporal variation in the phase of the acoustic signal, then any peaks in the spectrum will be related to the scale of turbulence which caused it (equation (51)).

An interesting note should be made here. The geometry of these experiments were very similar to those of Daigle et al. [10] The experiments Noble based his work on is over a larger variation of wind speeds and longer data collection times. Figure 11a is under similar wind conditions as Daigle et al. Looking at figure 11b, there is a spectral peak that appears at 2 Hz. That peak corresponded to turbulence on the order of 1.8 m. This is the scale of turbulence that Daigle observed in his results.

A model based on a vortex eddy pair was developed to model the wind flow variations. The wind field of the vortex eddy pair was calculated using the stream function:

$$f(x,z) = A\left[\cos(lx) + e^{-l^2/\alpha_x^2}\right]e^{-\alpha^2 r^2/4} \tag{56}$$

where

A	=	a constant specifying the intensity of the eddy pair
$\alpha^2 r^2$	=	$\alpha_x^2 x^2 + \alpha_z^2 z^2$
l	=	the characteristic wave number for the eddy pair
α_x	=	the horizontal wave numbers for the eddy pair
α_z	=	the vertical wave numbers for the eddy pair.

The coordinates (x,z) are relative to the center of the eddy pair. Townsend uses a characteristic wave number for the eddy pair of $\pi\alpha_x$. [27]

The horizontal velocity distribution can be calculated from the stream function using

$$u(x,z) = -\frac{\partial f(x,z)}{\partial z}. \tag{57}$$

Substituting equation (56) into equation (57) and carrying out the differentiation results in

$$u(x,z) = \frac{A\,\alpha_z^2 z}{2}\left[\cos(lx) + e^{-l^2/\alpha_x^2}\right]e^{-\alpha^2 r^2/4}. \tag{58}$$

Equation (58) provides the variations in the horizontal wind speed contributed by the presence of a large vortex pair. Where Roth's model deals with the fluctuations in the sound speed profile only with height, this model predicts the fluctuations of the sound speed profile in height and range.

Viewing the movement of the eddy pair on the geometric scales less than a few hundred meters in range, the variation of the speed of sound in the atmosphere would appear to change slowly over the entire range of the experiment uniformly. The expected phase change can be calculated using a simple model of the wind speed in the atmosphere slowly varying from v_1 to v_2:

$$\Delta \varphi = \frac{2\pi f R}{c_o^2}(v_1 - v_2) \tag{59}$$

where

R   =   the propagation distance

c_o =   the sound speed at temperature T

f   =   the frequency of the signal.

A comparison between the magnitude of the phase change for the simple model and experimental results are shown in table 5.

Table 5. Results from the simple model compared to measure data

Frequency (Hz)	$\Delta\varphi_{mea}$(degrees)	$\Delta\varphi_{pred}$(degrees)
62.5	40°	41°
125	72°	82°
250	155°	163°

For longer ranges, the simple phase model breaks down because the size of the eddy pair causes more influence on varying the speed of sound with range. A more complex model was developed to incorporate these range variations. The more complex model uses a PE [26] combined with the vortex eddy pair model. This model allows a refractive sound speed profile to be used with variations of the sound speed profile with height and range according to equation (58). The eddy pair is started out of the field of propagation and slowly stepped through the propagation field at the mean wind speed. At each step, the PE is run to calculate the phase and amplitude of the acoustic field at the receiver location. The current version of the model only takes into account the passage of one eddy pair. Unfortunately, there is no experimental data available for long propagation ranges. A comparison was made with the shorter range phase data. Tables 6 and 7 show the predicted phase output of the model compared with experimental measurements. Table 6 shows the comparison under low wind speed conditions, mean of approximately 3 m/s. This condition was used in the comparison, table 5, with the simple phase

model described earlier. Table 7 shows the comparison under high wind speed conditions, mean of approximately 10 m/s. The model works very well for the low and high wind speed conditions.

Table 6. **Comparison between large-scale eddy PE and data under low-wind conditions**

Frequency (Hz)	$\Delta\varphi_{mea}$(degrees)	$\Delta\varphi_{pred}$(degrees)
62.5	40°	42°
125	72°	83°
250	155°	169°

Table 7. **Comparison between large-scale eddy PE and data under high-wind conditions**

Frequency (Hz)	$\Delta\varphi_{mea}$(degrees)	$\Delta\varphi_{pred}$(degrees)
62.5	290°	289°
125	400°	400°
250	690°	704°

4. Conclusions and Future Models Work

This report has presented a brief overview of past and current turbulent scattering models and the impact on acoustic propagation. Until recently, the models available were crude and only valid for short ranges ($R \ll 1$ km). More advanced turbulence models have recently been devised for examining the effects of both large and small-scale turbulence on acoustic propagation in the atmosphere. Although the new models are more advanced, they provide only a partial answer to understanding the total effect of atmospheric turbulence on long range ($R > 10$ km) acoustic propagation in the atmosphere.

Most of the turbulence work conducted in atmospheric acoustics have concentrated on the small-scale turbulence or the turbulence in the Inertial Subrange of the Kolmogorov energy spectrum of atmospheric turbulence. The types of turbulence that primarily affect acoustic propagation in the atmosphere are thermal and mechanical turbulence. For short ranges, Daigle et al. used the work of Karavainikov, Chernov, and Tatarski to derive some relationships between scale size and turbulence strength for predicting mean fluctuations of the amplitude and phase of an acoustic signal for a given range. The more sophisticated acoustic propagation models, which incorporate a turbulence model, require large computers to perform the calculations for a scenario.

One of the latest advances in atmospheric acoustic propagation models is the Green's Function Parabolic Equation (GFPE). [28] The GFPE is a different formulation from the Crank-Nicolson PE, which performs calculations considerably faster. Work is being conducted to modify the turbulence model used in section 2.3.3 for the GFPE. This is not a straight forward derivation because the GFPE uses an FFT, which does not allow for a direct conversion of the turbulence model to the GFPE. Once the turbulence model is incorporated into the GFPE, an atmospheric acoustic propagation model that includes a turbulence model will be available, allowing calculations to be made within a reasonable time-frame on workstation sized computers.

The ultimate test of a computer model is to compare it to good quality field data. Most of the data available are for ranges less than 1 km. Some additional experiments need to be conducted with stable sources, not helicopters or tanks, out to ranges of 5 or 10 km. This will help to confirm the predictability of acoustic turbulence models at longer ranges.

References

1. Berry, F. A., Jr., E. Bollay, and N. A. Beers, *Handbook of Meteorology* McGraw-Hill Book Company, New York, 1945.

2. Panofsky, H. A., and J.A. Dutton, *Atmospheric Turbulence: Models and Methods For Engineering Applications*, Wiley, New York, 1984.

3. Monin, A. S., and A. M. Yaglom, *Statistical Fluid Mechanics: Mechanics of Turbulence*, MIT Press, Cambridge, 1975.

4. Chernov, L. A., *Wave Propagation In a Random Medium*, translated by R. A. Silverman, McGraw-Hill Book Company, New York, 1960.

5. Tatarski, V. I., *The Effects of Turbulent Atmosphere on Wave Propagation*, translated and published by Israel Programs for Scientific Translations Ltd., Jerusalem, 1971.

6. Karavainikov, V. N., "Fluctuations of Amplitude and Phase in a Spherical Wave," *Akust. Zh.* **3**: 175-186, 1975.

7. Daigle, G. A., J. E. Piercy, and T. F. W. Embleton, "Effects of Atmospheric Turbulence on the Interface of Sound Waves Near a Hard Boundary," *J. Acoust. Soc. Am.* **64**: 622-630, 1978.

8. De Wolf, D. A., "A Random-Motion Model of Fluctuations in a Nearly Transparent Medium," *Radio Sci.* **18**: 138-142, 1975.

9. Bass, Henry E., Lee N. Bolen, Richard Raspet, Walton McBride, and John Noble, "Acoustic Propagation Through a Turbulent Atmosphere: Experimental Characterization," *J. Acoust. Soc. Am.* **90**: 3307-3313, 1991.

10. Daigle, G. A., J. E. Piercy, and T. F. W. Embleton, "Line-of-Sight Propagation Through Turbulence Near the Ground," *J. Acoust. Soc. Am.* **74**: 1505-1513, 1983.

11. Taylor, G. I. "The Spectrum of Turbulence," *Proc. R. Soc. London A* **164**: 476-490, 1938.

12. McBride, Walton E., Henry E. Bass, Richard Raspet, and Kenneth E. Gilbert, "Scattering of Sound By Atmospheric Turbulence: A Numerical Simulation Above A Complex Impedance Boundary," *J. Acoust. Soc. Am.* **90**: 3314-3325, 1991.

13. McBride, Walton E., Henry E. Bass, Richard Raspet, and Kenneth E. Gilbert, "Scattering of Sound By Atmospheric Turbulence: Predictions in a Refractive Shadow Zone," *J. Acoust. Soc. Am.* **91**: 1336-1340, 1992.

14. Gilbert, Kenneth E., Richard Raspet, and Xiao Di, "Calculation of Turbulence Effects in an Upward-Refracting Atmosphere," *J. Acoust. Soc. Am.* **87**: 2428-2437, 1990.

15. Weiner, F. M., and D. N. Keast, "Experimental Study of the Propagation of Sound Over Ground," *J. Acoust. Soc. Am.* **31**: 724-733, 1959.

16. Auvermann, H. J., R. L. Reynolds, and D. M. Brown, "Development of a Multi-Stream Acoustic Propagation Model Including Turbulence Scattering," (Technical report in preparation), U.S. Army Research Laboratory, White Sands Missile Range, NM, 1993a.

17. Goedecke, G. H., and H. J. Auvermann, "Turbulence Acoustical Scattering Theory From the Structural Approach," (Technical report in preparation), U.S. Army Research Laboratory, White Sands Missile Range, NM, 1993c.

18. Rollins, C. J., D. G. Resendes, and M. R. Squillante, "Acoustic Scattering by a Vortex Model of Turbulence," (Contractor report in preparation), U.S. Army Research Laboratory, White Sands Missile Range, NM, 1993.

19. Raspet, R., S. W. Lee, E. Kuester, D. C. Chang, W. F. Richards, R. Gilbert, and N. Bong, "Fast-Field Program for a Layered Medium Bounded by Complex Impedance Surfaces," *J. Acoust. Soc. Am.* **77**: 343-352, 1985.

20. Lee, S. W., N. Bong, W. F. Richards, and R. Raspet, "Impedance Formulation of the Fast Field Program for Acoustic Wave Propagation in the Atmosphere," *J. Acoust. Soc. Am.* **79**: 628-634, 1986.

21. Pasquill, F., *Atmospheric Diffusion*, John Wiley & Sons, New York, 1974.

22. Rudnick, I., "Fluctuations in Intensity of an Acoustic Wave Transmitted Through a Turbulent Heated Lamina," *J. Acoust. Soc. Am.* **19**: 202-205, 1947.

23. Ingard, U., "A Review of the Influence of Meteorological Condition on Sound Propagation," *J. Acoust. Soc. Am.* **25**: 405-411, 1953.

24. Chessell, C. I., "Observations of the Effects of Atmospheric Turbulence on Low-Frequency Sound Propagation," *J. Acoust. Soc. Am.* **60**: 29-33, 1976.

25. Roth, S. D., "Acoustic Propagation in the Surface Layer Under Convectively Unstable Conditions," Ph.D. Dissertation, Pennsylvania State University, 1983.

26. Noble, John M., Henry E. Bass, and Richard Raspet, "The Effect of Large-Scale Atmospheric Inhomogeneities on Acoustic Propagation," *J. Acoust. Soc. Am.* **92**: 1040-1046, 1992.

27. Townsend, A. A., *The Structure of Turbulent Shear Flow*, Cambridge U.P., New York, 1976.

28. Marlin, Dave, "Fast Parabolic Approximations for Acoustic Propagation in the Atmosphere," (Technical report in preparation), U.S. Army Research Laboratory, White Sands Missile Range, NM, 1993.

Acronyms and Abbreviations

AMPP   Acoustic Multi-Stream Propagation Program

FFP   Fast Field Program

FFT   Fast-Fourier Transform

PBL   planetary boundary layer

PE   Parabolic Equation

TEM   Turbule Ensemble Model

Distribution

```
ARMY MISSILE CMND                                    1
AMSMI RD AS SS
ATTN MR B WILLIAMS
REDSTONE ARSENAL
AL 35898-5253

ARMY MISSILE CMND                                    1
AMSMI RD DE SE
ATTN MR GORDON LILL JR
REDSTONE ARSENAL
AL 35898-5245

ARMY MISSILE CMND                                    1
REDSTONE SCI INFO CTR
AMSMI RD CS R DOC
REDSTONE ARSENAL
AL 35898-5241

ARMY MISSILE CMND                                    1
AMSMI
REDSTONE ARSENAL
AL 35898-5253

ARMY INTEL CTR                                       1
AND FT HUACHUCA
ATSI CDC C
FT HUACHUCA AZ 85613-7000

NORTHROP CORPORATION                                 1
ELECTR SYST DIV
ATTN MRS T BROHAUGH
2301 W 120TH ST BOX 5032
HAWTHORNE CA 90251-5032

NAVAL WEAPONS CTR                                    1
CODE 3331
ATTN DR SHLANTA
CHINA LAKE CA 93555
```

PACIFIC MISSILE TEST CTR   1
GEOPHYSICS DIV
ATTN CODE 3250
POINT MUGU CA 93042-5000

LOCKHEED MIS & SPACE CO   1
ATTN KENNETH R HARDY
ORG 91 01 B 255
3251 HANOVER STREET
PALO ALTO CA 94304-1191

NAVAL OCEAN SYST CTR   1
CODE 54
ATTN DR RICHTER
SAN DIEGO CA 92152-5000

METEOROLOGIST IN CHARGE   1
KWAJALEIN MISSILE RANGE
PO BOX 67
APO SAN FRANCISCO
CA 96555

DEPT OF COMMERCE CTR   1
MOUNTAIN ADMINISTRATION
SPPRT CTR LIBRARY R 51
325 S BROADWAY
BOULDER CO 80303

DR HANS J LIEBE   1
NTIA ITS S 3
325 S BROADWAY
BOULDER CO 80303

NCAR LIBRARY SERIALS   1
NATL CTR FOR ATMOS RSCH
PO BOX 3000
BOULDER CO 80307-3000

DEPT OF COMMERCE CTR   1
325 S BROADWAY
BOULDER CO 80303

DAMI POI   1
WASH DC 20310-1067

MIL ASST FOR ENV SCI OFC   1
OF THE UNDERSEC OF DEFNS
FOR RSCH & ENGR R&AT E LS
PENTAGON ROOM 3D129
WASH DC 20301-3080

DEAN RMD   1
ATTN DR GOMEZ
WASH DC 20314

SPACE NAVAL WARFARE   1
SYST CMND
PMW 145 1G
WASH DC 20362-5100

ARMY INFANTRY   1
ATSH CD CS OR
ATTN DR E DUTOIT
FT BENNING GA 30905-5090

AIR WEATHER SERVICE   1
TECH LIBRARY FL4414 3
SCOTT AFB IL 62225-5458

USAFETAC DNE   1
ATTN MR GLAUBER
SCOTT AFB IL 62225-5008

HQ AWS DOO 1   1
SCOTT AFB IL 62225-5008

ARMY SPACE INSTITUTE   1
ATTN ATZI SI 3
FT LEAVENWORTH
KS 66027-5300

PHILLIPS LABORATORY   1
PL LYP
ATTN MR CHISHOLM
HANSCOM AFB MA 01731-5000

ATMOSPHERIC SCI DIV   1
GEOPHYSICS DIRCTRT
PHILLIPS LABORATORY
HANSCOM AFB MA 01731-5000

PHILLIPS LABORATORY   1
PL LYP 3
HANSCOM AFB MA 01731-5000

RAYTHEON COMPANY   1
ATTN DR SONNENSCHEIN
528 BOSTON POST ROAD
SUDBURY MA 01776
MAIL STOP 1K9

ARMY MATERIEL SYST   1
ANALYSIS ACTIVITY
AMXSY
ATTN MP H COHEN
APG MD 21005-5071

ARMY MATERIEL SYST   1
ANALYSIS ACTIVITY
AMXSY AT
ATTN MR CAMPBELL
APG MD 21005-5071

ARMY MATERIEL SYST   1
ANALYSIS ACTIVITY
AMXSY CR
ATTN MR MARCHET
APG MD 21005-5071

ARL CHEMICAL BIOLOGY   1
NUC EFFECTS DIV
AMSRL SL CO
APG MD 21010-5423

ARMY MATERIEL SYST   1
ANALYSIS ACTIVITY
AMXSY
APG MD 21005-5071

NAVAL RESEARCH LABORATORY   1
CODE 4110
ATTN MR RUHNKE
WASH DC 20375-5000

ARMY MATERIEL SYST   1
ANALYSIS ACTIVITY
AMXSY CS
ATTN MR BRADLEY
APG MD 21005-5071

ARMY RESEARCH LABORATORY   1
AMSRL D
2800 POWDER MILL ROAD
ADELPHI MD 20783-1145

ARMY RESEARCH LABORATORY   1
AMSRL OP SD TP
TECHNICAL PUBLISHING
2800 POWDER MILL ROAD
ADELPHI MD 20783-1145

ARMY RESEARCH LABORATORY   1
AMSRL OP CI SD TL
2800 POWDER MILL ROAD
ADELPHI MD 20783-1145

ARMY RESEARCH LABORATORY 1
AMSRL SS SH
ATTN DR SZTANKAY
2800 POWDER MILL ROAD
ADELPHI MD 20783-1145

ARMY RESEARCH LABORATORY 1
AMSRL
2800 POWDER MILL ROAD
ADELPHI MD 20783-1145

NATIONAL SECURITY AGCY W21 1
ATTN DR LONGBOTHUM
9800 SAVAGE ROAD
FT GEORGE G MEADE
MD 20755-6000

ARMY AVIATION CTR 1
ATZQ D MA
ATTN MR HEATH
FT RUCKER AL 36362

OIC NAVSWC 1
TECH LIBRARY CODE E 232
SILVER SPRINGS
MD 20903-5000

ARMY RSRC OFC 1
ATTN DRXRO GS
PO BOX 12211
RTP NC 27009

DR JERRY DAVIS 1
NCSU
PO BOX 8208
RALEIGH NC 27650-8208

ARMY CCREL 1
CECRL GP
ATTN DR DETSCH
HANOVER NH 03755-1290

ARMY ARDEC   1
SMCAR IMI I BLDG 59
DOVER NJ 07806-5000

ARMY COMMUNICATION   1
ELECTR CTR FOR EW RSTA
AMSEL RD EW SP
FT MONMOUTH NJ 07703-5206

ARMY SATELLITE COMM AGCY   1
DRCPM SC 3
FT MONMOUTH NJ 07703-5303

ARMY COMMUNICATIONS   1
ELECTR CTR FOR EW RSTA
AMSEL EW D
FT MONMOUTH NJ 07703-5303

ARMY COMMUNICATIONS   1
ELECTR CTR FOR EW RSTA
AMSEL EW MD
FT MONMOUTH NJ 07703-5303

ARMY DUGWAY PROVING GRD   1
STEDP MT DA L 3
DUGWAY UT 84022-5000

ARMY DUGWAY PROVING GRD   1
STEDP MT M
ATTN MR BOWERS
DUGWAY UT 84022-5000

DEPT OF THE AIR FORCE   1
OL A 2D WEATHER SQUAD MAC
HOLLOMAN AFB
NM 88330-5000

PL WE   1
KIRTLAND AFB NM
87118-6008

USAF ROME LAB TECH   1
CORRIDOR W STE 262 RL SUL
26 ELECTR PKWY BLD 106
GRIFFISS AFB
NY 13441-4514

AFMC DOW   1
WRIGHT PATTERSON AFB
OH 0334-5000

ARMY FIELD ARTLLRY SCHOOL   1
ATSF TSM TA
FT SILL OK 73503-5600

NAVAL AIR DEV CTR   1
CODE 5012
ATTN AL SALIK
WARMINISTER PA 18974

ARMY FOREGN SCI TECH CTR   1
CM
220 7TH STREET NE
CHARLOTTESVILLE
VA 22901-5396

NAVAL SURFACE WEAPONS CTR   1
CODE G63
DAHLGREN VA 22448-5000

ARMY OEC   1
CSTE EFS
PARK CENTER IV
4501 FORD AVE
ALEXANDRIA VA 22302-1458

ARMY CORPS OF ENGRS   1
ENGR TOPOGRAPHICS LAB
ETL GS LB
FT BELVOIR VA 22060

TAC DOWP
LANGLEY AFB
VA 23665-5524   1

ARMY TOPO ENGR CTR
CETEC ZC 1
FT BELVOIR VA 22060-5546   1

LOGISTICS CTR
ATCL CE
FT LEE VA 23801-6000   1

SCI AND TECHNOLOGY
101 RESEARCH DRIVE
HAMPTON VA 23666-1340   1

ARMY NUCLEAR CML AGCY
MONA ZB BLDG 2073
SPRINGFIELD VA 22150-3198   1

ARMY FIELD ARTLLRY SCHOOL
ATSF F FD
FT SILL OK 73503-5600   1

USATRADOC
ATCD FA
FT MONROE VA 23651-5170   1

ARMY TRADOC ANALYSIS CTR
ATRC WSS R
WSMR NM 88002-5502   1

ARMY RESEARCH LABORATORY
AMSRL BE M
BATTLEFIELD ENVIR DIR
WSMR NM 88002-5501   1

ARMY RESEARCH LABORATORY
AMSRL BE A
BATTLEFIELD ENVIR DIR
WSMR NM 88002-5501   1

ARMY RESEARCH LABORATORY   1
AMSRL BE W
BATTLEFIELD ENVIR DIR
WSMR NM 88002-5501

ARMY RESEARCH LABORATORY   1
AMSRL BE
ATTN MR VEAZEY
BATTLEFIELD ENVIR DIR
WSMR NM 88002-5501

DEFNS TECH INFO CTR   1
CENTER DTIC BLS
BLDG 5 CAMERON STATION
ALEXANDRIA
VA 22304-6145

ARMY COMMUNICATIONS   1
ELECTR CTR FOR EW RSTA
AMSEL
FT MONMOUTH NJ 07703-5303

ARMY MISSILE CMND   1
AMSMI
REDSTONE ARSENAL
AL 35898-5243

ARMY DUGWAY PROVING GRD   1
STEDP 3
DUGWAY UT 84022-5000

ARMY COMMUNICATIONS   1
ELECTR CTR FOR EW RSTA
AMSEL
FT MONMOUTH NJ 07703-5206

USATRADOC   1
ATCD FA
FT MONROE VA 23651-5170

ARMY FIELD ARTLRY SCHOOL   1
ATSF
FT SILL OK 73503-5600

WSMR TECH LIBRARY BR   1
STEWS IM IT
WSMR NM 88001

Record Copy   10

TOTAL   99